CHAPTER II
THEORETICAL BACKGROUND AND LITERATURE SURVEY

2.1 Natural Gas

Natural gas is generally considered a non-renewable fossil fuel. It is believed that natural gas was formed from the remains of tiny sea animals and plants, buried by the layers of sediment that turn to rock 200 – 400 million years ago. Over the years, the layers of sedimentary rock became a thousand feet of thickness, causing the energy-rich plant and animal remains to enormous pressure, and transforming their constituent compounds into a mixture of alkanes. Natural gas is formed in deep underground, usually in areas around coal and oil. It is composed mostly of methane, but also contained other chemical species, such as butane and propane. Natural gas might also contain non-hydrocarbon compounds, such as water vapor, carbon dioxide, and hydrogen sulfide. It is one of the most widely used forms of energy in recent year. Natural gas is a cleaner-burning fuel than gasoline and diesel. However, it also contains active and inert compounds, such as sulfur, nitrogen, and carbon dioxide. However, the combustion of natural gas is clean and emits less CO_2 than all other petroleum derivative fuels, which makes it favorable in terms of the greenhouse effect. Natural gas is used across all sectors, in varying amounts, including in industrial, residential, electricity generation, commercial, and transportation sectors (Demirbas, 2010).

Over the next 20 years, the role of natural gas in global energy consumption will increase substantially. The speed of the transition to natural gas will be driven by environmental constraints, increased demand, and new technologies. A potential source of natural gas lies in the enormous worldwide gas hydrate reserves. However, these deposits can cause problems and safety concerns relating to drilling, production of oil and gas, and building or operation of pipelines. Naturally occurring gas hydrates are normally found at the seafloor or in shallow sediments where the pressures and temperatures are conducive to hydrate formation (Demirbas, 2010).

2.2 Natural Gas Hydrates

The existence of natural gas hydrates was first identified by Sir Humphrey Davy in 1810 through the formation of chlorine hydrate in the laboratory (Davy, 1811). Gas hydrates remained as curiosity of only academic interest until Hammerscmidt discovered the hydrate that caused the gas transmission pipeline blockage in 1934, turning the attention of research interest on gas hydrate formation and prevention as it nuisance for the oil and gas production industry (Hammerschmidt, 1934). Since then, hydrate research has been intensified especially after the discovery of natural gas hydrate deposits in the Siberian permafrost regions by Makogon in 1965 (Makogon, 1981).

Natural gas hydrates, primary composed of methane are non-stoichiometric, crystalline substances formed by water and light natural gases. In the molecules of hydrate, gas molecules are entrapped in the water lattice formed by hydrogen bonds. The lattice is composed of cavities of various sizes that occupied by the gas molecules, and the gas molecules are bound in the lattice through weak van der Waals forces (Englezos, 1993; Sloan and Koh, 2008). The given favorable condition of high pressure and low temperature in addition to the availability of free methane and water, gas hydrates can form and remain stable (Englezos, 1993; Sloan and Koh, 2008). Such conditions can exist in ocean-bottom sediments at water depths below 500 m (Kvenvolden 1993). Methane is the dominant component among other hydrocarbon gases in sediments, so that the terms "methane hydrate" and "gas hydrate" are often used interchangeably, and refer to the methane–water crystalline structure called a clathrate (Mazzini *et al.* 2004; Popescu *et al.* 2006; Demirbas, 2010).

In fact, numerous field studies have shown that gas hydrate is widespread in permafrost regions and beneath the sea in sediments of outer continental margins (Figure 2.1). Natural gas hydrates have the potential to provide an enormous resource of natural gas from the world's oceans and the polar regions. Figure 2.2 shows phase diagram of methane hydrate stability zone at different depth-temperature. The hydrate formation requirements restrict the occurrence of natural gas hydrates to two types of geologic locations: a) under permafrost in the polar continental shelves and

b) in sediment beneath the ocean floor (Allison, 2008). As seen from the figure, the hydrate deposits themselves may be several hundred meters thick. The resource contained in marine methane hydrate deposits is significantly larger and occurs in many more countries than do Arctic hydrates (Allison, 2008).

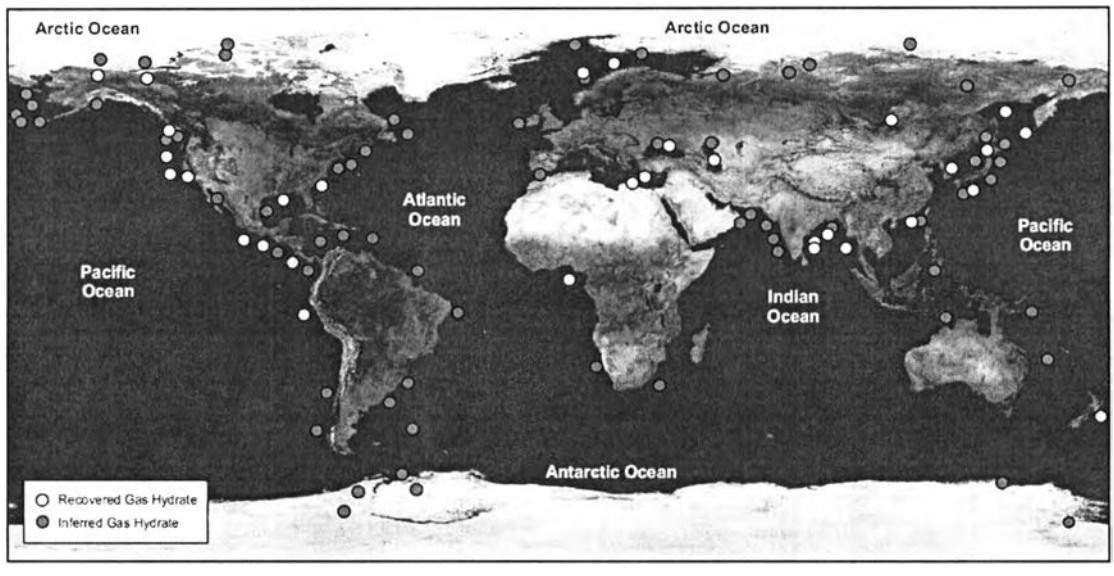

Figure 2.1 Location of sampled and inferred gas-hydrate occurrences in oceanic sediments of outer continental margins and permafrost regions (modified from Kvenvolden, 1993).

The global estimates of the methane hydrate resource vary considerably, from 1×10^{15} to 5×10^{15} m^3 at STP to 21×10^{15} m^3 (Kvenvolden, 1999; Milkov, 2004). This is significantly larger than the estimate of global conventional natural gas resources of 44×10^{13} m^3 (US Geological Survey, 2000). The methane hydrate estimates are for gas in-place. Actual production would be only a percentage of this volume. However, the potentially producible volume could still be larger than with conventional natural gas resources (Allison, 2008). This volume of natural gas contained in the world's gas hydrate accumulations is generally accepted to greatly exceed that of known gas reserves (Collett, 2002). However, according to the recent National Research Council (United States) report on methane hydrates, there are no fundamental technological hurdles to recovering energy from these natural deposits, although more research needs to be performed to determine the environmental

impact of such exploration (Koh *et al.*, 2011).

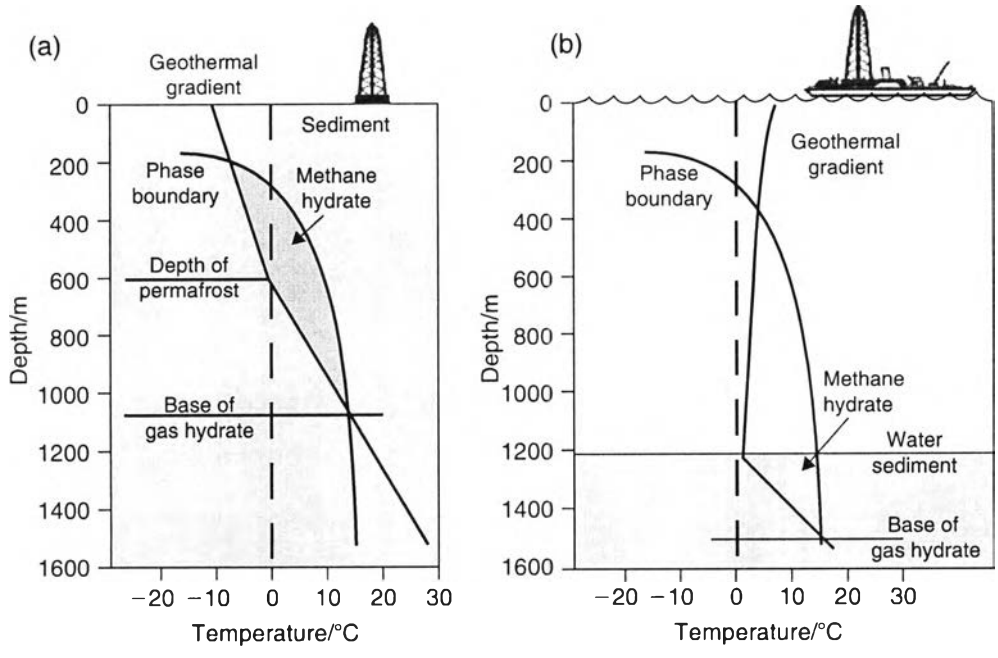

Figure 2.2 Phase diagram of methane hydrate stability zone at different depth-temperature: (a) permafrost and (b) oceanic environment (Allison, 2008).

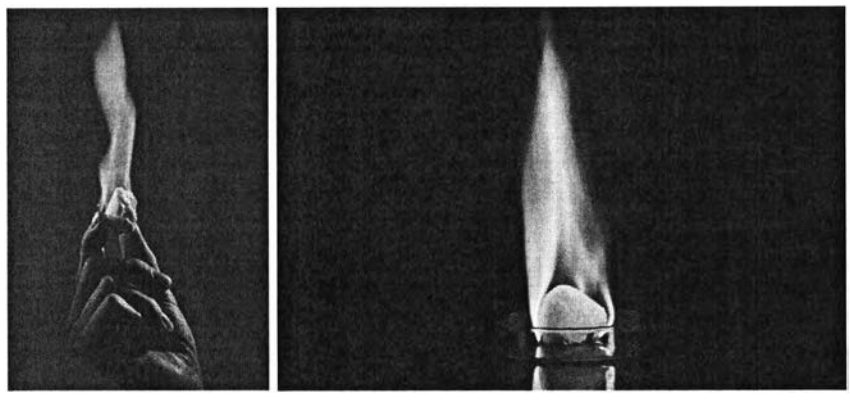

Figure 2.3 Methane hydrate samples (ngm.nationalgeographic.com, www.bloomberg.com).

As can be seen from Figure 2.3, methane gas hydrate samples easily burn under atmospheric pressure. If methane hydrate is warmed or depressurized, it can be reverted back to water and natural gas. Although the global estimates vary considerably, the energy content of methane occurring in hydrate form is immense,

possibly exceeding the combined energy content of all other known fossil fuels (Demirbas, 2010).

Gas hydrates are crystalline compounds that result from the three dimensional (3-D) stacking of cages of hydrogen-bonded water molecules (Sloan and Koh, 2008). Commonly, the cage can hold a single gas molecule, as shown in Figure 2.4. Gas hydrates are clathrates, meaning that guest gas molecules are encaged in a host framework of water molecules. The empty cagework is unstable and requires the presence of encapsulated gas molecules to stabilize the clathrate crystal. The compact nature of the hydrate structure makes for a highly effective packing of gas. A volume of gas hydrate expands between 150 and 180 fold when released in gaseous form at standard pressure and temperature (1 kPa, 208 °C) (Sloan and Koh, 2008).

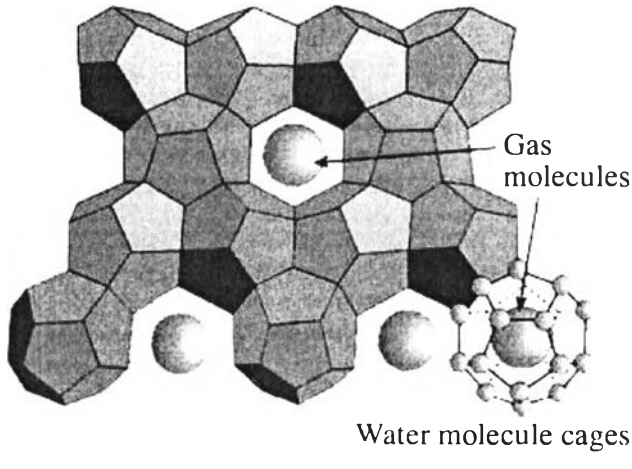

Figure 2.4 Water ice-like cage structure of gas hydrate (Demirbas, 2010).

2.3 Gas Hydrate Structures

Gas hydrates are known as non-stoichiometric compounds because some of the cages in the structure can be vacant; however, a sufficient number of cages must be occupied by gas molecules to stabilize the hydrate crystals. In general, there is a maximum of one guest per cage, except under high pressure conditions (>0.1 GPa) when multiple occupancies of large cages can occur (Koh *et al.*, 2011). The

crystalline structure is composed of polyhedra of hydrogen-bonded water molecules. The cages formed by polyhedra contain at most one guest molecule per each. The cages are stabilized by van der Waals forces between the water molecules and the encapsulated guest molecule (Sloan and Koh, 2008).

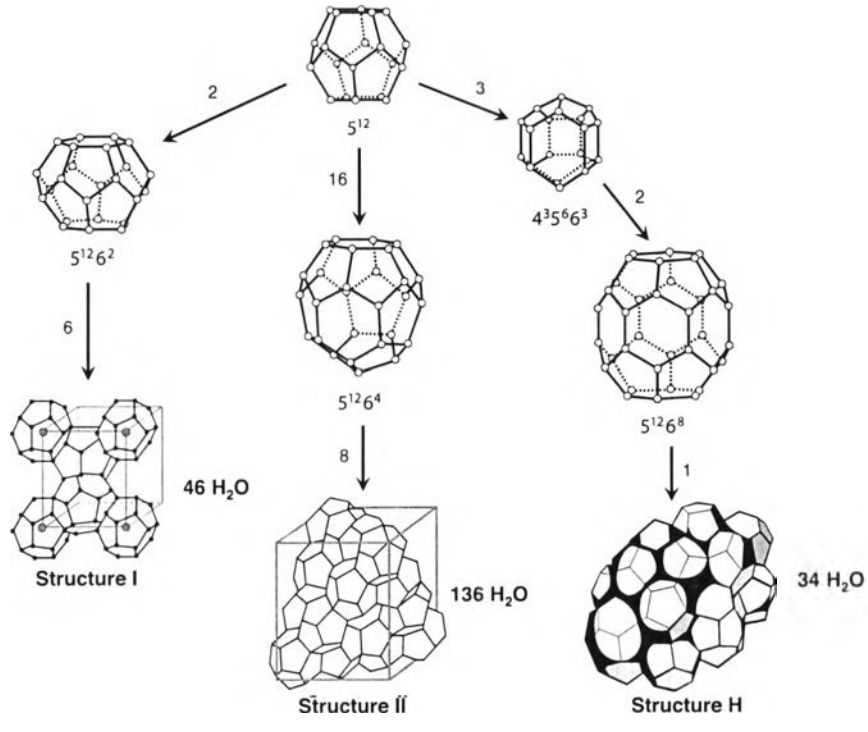

Figure 2.5 Common gas hydrate structure (sI, sII, and sH) and the water cage types that compose the hydrate structures (modified from Koh *et al.*, 2011).

Table 2.1 Geometry of hydrate unit cells and cavities (modified from Sloan and Koh, 2008)

Structure	**I**		**II**		**H**		
Crystal system	Cubic		Cubic		Hexagonal		
Number of H_2O molecules	46		136		34		
Cavity	Small	Large	Small	Large	Small	Medium	Large
Description	5^{12}	$5^{12}6^2$	5^{12}	$5^{12}6^4$	5^{12}	$4^35^66^3$	$5^{12}6^8$
Number of cavities/unit cell	2	6	16	8	3	2	1
Avg. cavity radius (Å)	3.95	4.33	3.91	4.73	3.94	4.04	5.79
Variation in radius (%)	3.4	14.4	5.5	1.73	4.0	8.5	15.1
Coordination number	20	24	20	28	20	20	36

There are three main types of gas hydrate crystal structures, which are known as structure I (sI), structure II (sII), and structure H (sH), as shown in Figure 2.5 (Sloan and Koh, 2008). The number of water molecules, cages, and some geometry of the different hydrate structures are given in Table 2.1.

2.3.1 Structure I (sI)

Structure I is the structure with the simplest hydrate structure and has a cubical shape. It consists of two types of cavities such as dodecahedron and tetrakaidecahedron, as seen in Figure 2.6. The dodecahedron is a 12-sided polyhedron where each face is a pentagon twelve edge 5^{12}, which is the smallest of the cavities. It contains 20 molecules of water with 30 hydrogen bonds, and has a radius of 3.95 Å. At a normal temperature and pressure, the cavities may contain CH_4, N_2, H_2S, H_2, Kr, Ar, and the other non-polar gas molecules. Tetrakaidecahedron is a 14-sided polyhedron with 12 pentagonal and two hexagonal side faces, $5^{12}6^2$. This large cavity containing 26 water molecules and has a radius of 4.33 Å. The cavities can contain including carbon dioxide and ethane. Methane can occupy both the small and large cavities, while ethane can only occupy the large. (Sloan and Koh, 2008)

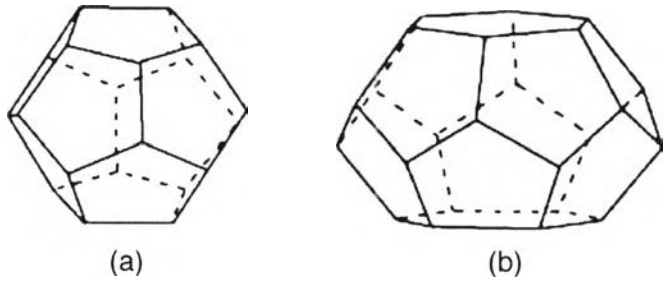

Figure 2.6 Structure I gas hydrate crystal structure: a) pentagonal dodecahedron and b) tetrakaidecahedron (modified from Demirbas, 2010).

A unit sI hydrate cell contains 46 molecules of water arranged in lattice around 8 cavities. Of these eight cavities 2 of them are small and 6 of them large. (Sloan and Koh, 2008; Koh *et al.*, 2011).

2.3.2 Structure II (sII)

Structure II is more complex than structure I, but still has a cubical shape. It also consists of small and large cavities. Figure 2.7 shows the hydrate crystal structures in structure II hydrate such as hexsakaidecahedron and dodecahedron. The dodecahedron has exactly the same shape as that of sI, a 12-sided polyhedron where each face is a pentagon twelve edge, 5^{12}. The hexsakaidecahedron is a 16-sided polyhedron with twelve pentagonal side surfaces and four hexagonal side faces, $5^{12}6^4$. The larges cavities of the sII are bigger than the large cavity of sI, and can accommodate larger guest molecules (Sloan and Koh, 2008; Koh *et al.*, 2011). The small cavity of sII has cavity radius slightly less than sI as indicated by Table 2.1. In contrast, sI unit cell has 46 water molecules, while the unit cell of sII has 136 water molecules, arranged in lattice of 24 cavities, 16 small and 8 large. The most common sII hydrate formers are propane and iso-butane, which only occupy the large cavity. Structure II is the most common structure that formed in oil and the gas industry. This is also the most stable structure (Sloan and Koh, 2008).

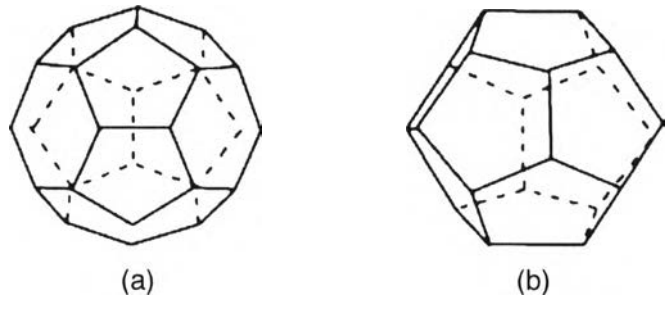

Figure 2.7 Structure II gas hydrate crystal structure: a) hexakaidecahedron and b) dodecahedron (modified from Demirbas, 2010).

2.3.3 Structure H (sH)

The third and last identified structure is structure H, identified by Ripmeester in 1987 (Ripmeester *et al.* 1987). H stands for hexagonal, which is the shape of the structure. SH consists of small, medium and large cavities as present in Figure 2.8. It occurs much less frequently than the other two, and in terms of stability it lies between sI and sII.

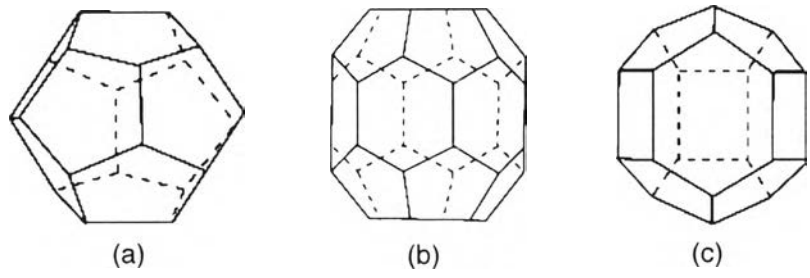

Figure 2.8 Structure H gas hydrate crystal structure: a) pentagonal dodecahedron, b) icosahedron, and b) irregular dodecahedron (modified from Demirbas, 2010).

Structure H requires two types of guest molecules to stabilize the hydrate structure; one help gas that fits into the small and medium cavities, and the structure H former that fits in the large cavities (Ripmeester *et al.* 1987). The small cavity is still the dodecahedron, while the medium sized cavity is an irregular dodecahedron consisting of 4-square sides, six pentagonal lateral surfaces and three hexagonal sides, $4^3 5^6 6^3$, which has a radius of 4.06 Å. The large cavity is an irregular isocahedron, a 20-sided polyhedron with 12 pentagonal and 8 hexagonal side faces, $5^{12} 6^8$, with a radius of 5.71 Å (Sloan and Koh, 2008). The unit cell of sH consists of 34 water molecules, arranged in 3 small, 2 medium and 1 large cavities.

The sI and sII may be formed in the presence of only one hydrate forming gas only, while structure H requires a help gas such as methane to form the structure. These structure H rarely occurs in natural gas, and this could be the reason why sH occurs less frequently than sI and sII (Carroll, 2003).

2.4 Gas Hydrate Formation Process

Figure 2.9 presents an example of hydrate nucleation and growth, considering the gas consumption versus time trace in the agitated system, operated at constant pressure and temperature. An autoclave cell, containing water is pressurized with gas and brought to the hydrate formation conditions (P, T). The gas is introduced from the reservoir to maintain constant pressure as hydrates form with time. The rate of gas consumption is the hydrate formation rate that can be controlled

by kinetics, or heat or mass transfer (Sloan and Koh, 2008).

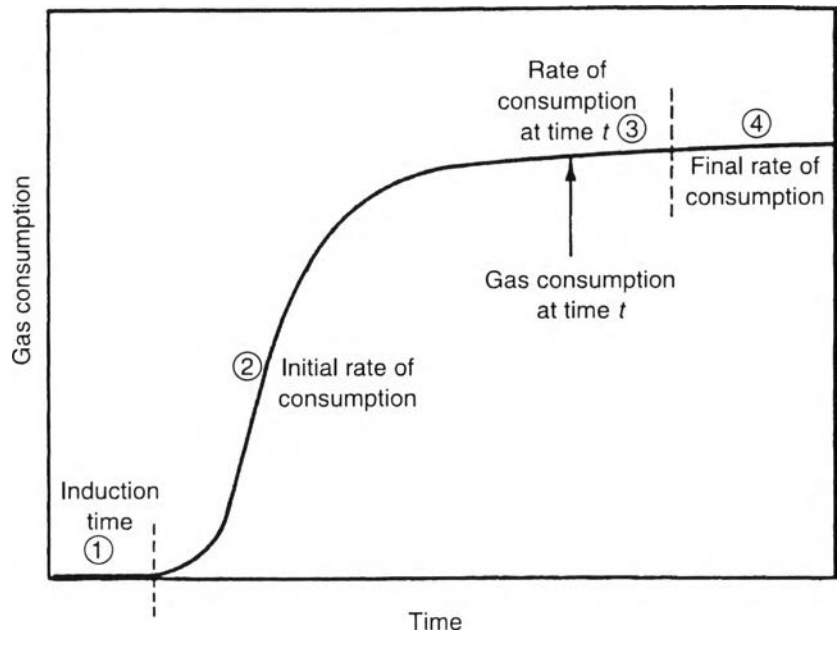

Figure 2.9 Gas consumption versus time for hydrate formation (Sloan and Koh, 2008).

The induction time is marked as 1 and includes the time taken for the hydrate crystal to form. The induction time is defined in practice as the time elapsed until the appearance of a detectable volume of hydrate phase or equal to the consumption of a detectable number of moles of hydrate former gas. The induction time is often also termed the hydrate nucleation or lag time (Sloan and Koh, 2008).

During the induction period, the temperature and pressure conditions are within the hydrate stable region. However, the hydrate does not form within this period because of the metastability, which is the ability of a non-equilibrium state to persist for a long period of time. The growth period in region 2 indicates a very rapid hydrate growth occurs. During the growth period, gas is being concentrated in the hydrate cages—hydrated gas molecules are more densely packed than those in the vapor. As the water is consumed by hydrate formation, the slope of the gas consumption trace eventually decreases with time (Points 3-4) (Sloan and Koh, 2008).

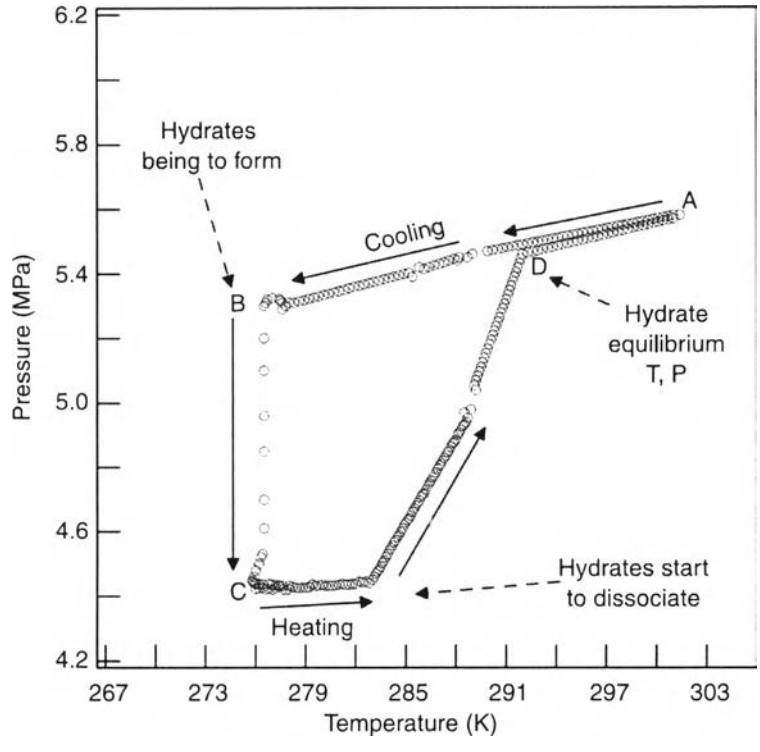

Figure 2.10 Temperature and pressure trace for simple methane hydrates formation (Sloan and Koh, 2008).

An alternative hydrate formation and dissociation experiment is shown in the temperature and pressure trace of Figure 2.10. In this case, the volume is constant and the temperature is changed during the experiment. In the experiment, the apparatus consists of the agitated autoclave cell, housing a sight glass window contains water that is pressurized with methane gas to the upper rightmost temperature and pressure in the close system. As the cell temperature is lowered, the pressure decreases, principally due to gas contraction as well as increased gas solubility upon cooling at constant volume (Sloan and Koh, 2008).

The metastability of the system prevents the hydrate forming immediately at Point D, which is attributed to the hydrate equilibrium point, as seen in Figure 2.10. Instead the system pressure continues to decrease linearly with temperature for several hours, without hydrate formation occurring (A to B is the induction period, Point 1 in Figure 2.9). At Point B, the hydrates begin to form. The pressure drops rapidly to Point C (about 1.01 MPa or 10 atm in 0.5 h). B to C is the catastrophic

growth period (Point 2 in Figure 2.9).

Hydrate dissociation begins when the cell is heated from Point C in Figure 2.10, so that the system pressure increases, at first slowly and then sharply along the steep dissociation line (between Points C and D). Finally at Point D, the hydrates are completely dissociated, as confirmed visually through the sight glass. The hydrate equilibrium condition (or hydrate dissociation temperature and pressure) is given by Point D (Sloan and Koh, 2008).

Usually 1 – 2 days (for reactors on this scale, 300 cm^3) of the experimental effort are required to traverse the loop as shown in Figure 2.10. In order to avoid obtaining an erroneous dissociation temperature and pressure, the dissociation part of the loop must be performed at a sufficiently slow heating rate at about 0.12 K/h to allow the system to reach equilibrium (Tohidi *et al.*, 2000; Rovetto *et al.*, 2006). The different temperature between Point D to that at Point B is called the subcooling (more properly the supercooling, ΔT_{sub}, where $\Delta T_{sub} = T_{eqm}$ (D)$-T$(B) (Sloan and Koh, 2008).

As illustrated in Figure 2.10, there is a fundamental difference in hydrate initiation and dissociation due to the associated gas and liquid phases being disorderly on a molecular level, while the hydrate crystals are orderly in nature. Entropy favors disorder over order, so the initial hydrate formation is hindered by a metastable period (induction period). During this period, the disorderly gas and liquid water begin to rearrange into the orderly hydrate crystal structure. Conversely, dissociation begins relatively rapidly after the hydrate is removed from the temperature and pressure stability region (Sloan and Koh, 2008).

2.4.1 Hydrate Nucleation Kinetics

Nucleation is probably the most challenging step in the understanding of the process of gas hydrate formation. Hydrate nucleation is a process where small sub-critical embryonic clusters of water and gas continuously form and dissociates in an attempt to achieve a critical size for sustainable hydrate growth. The region where the formation and dissolution of such embryonic pre-hydrate structures occurs, with equal probability, is called a metastable region (Sloan and Koh, 2008). On a micro scale this process involves between ten and a thousand molecules; thus, it is very

difficult to observe experimentally. Currently. the hypotheses for hydrate nucleation are based on the known phenomena such as freezing water, gas dissolution in water and simulated data of both phenomena (Sloan and Koh, 2008).

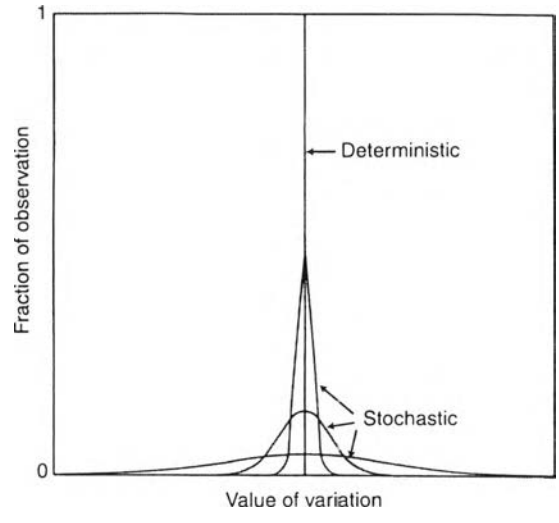

Figure 2.11 Comparison of stochastic and deterministic properties (Rowley, 1994; Sloan and Koh, 2008)

Nucleation processes are in general stochastic. The difference between stochastic and deterministic features is illustrated in Figure 2.11. For a specific equilibrium state, the probability of observing a particular condition at given temperature is 1. The deterministic equilibrium condition involves negligible variation in the measured temperature. Stochastic behavior is evidenced in the three lower curves in Figure 2.11 (Sloan and Koh, 2008).

Considering at the results from hydrate nucleation experiments in the laboratory, the stochastic behavior or the width of the variation, as illustrated in Figure 2.11, is the function of experimental temperature. At the temperatures close to the equilibrium, the distribution width of measured nucleation times may be very broad and appear as very stochastic, while at lower temperatures nucleation occurs more frequently and the process occurs as apparently less stochastic on the time scale.

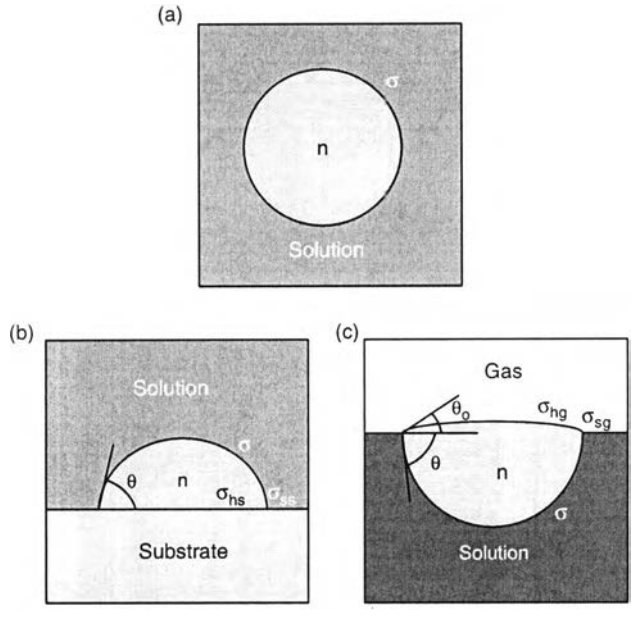

Figure 2.12 Schematic of (a) spherical cluster of building devices is homogeneous, (b) hat-shaped cluster of n building units in 3D in heterogeneous on a substrate, (c) Lens-shaped cluster of n building units in 3D in heterogeneous the solution gas interface (Sloan and Koh, 2008).

Primary nucleation can be a homogenous or heterogeneous type. The homogeneous nucleation occurs spontaneously in the solution and involves two phases only – the solution and the new phase being formed in the solution. This behavior is illustrated in Figure 2.12a. The heterogeneous nucleation involves three or more phases and occurs at the interface between gas, water, and the forming hydrate (the new phase) as illustrated in Figure 2.12c. The heterogeneous nucleation may also occur on the surface of a foreign particle, which is added to the solution, at a metal surface or on the surface of a substrate as illustrated in Figure 2.12b. The substrate will act as the third phase involved in the nucleation process (Sloan and Koh, 2008).

2.4.2 Hydrate Crystal Growth Processes

There are different types of hydrate crystal growth processes. It can be divided into four main types (Sloan and Koh, 2008): (1) Single crystal growth, (2)

Hydrate film/shell growth at the water-hydrocarbon interface, (3) Multiple crystal growth in an agitated system, and (4) Growth of metastable phases. Type (1) and type (2) processes are most relevant to this study. Therefore, in the next two sections, the single crystal growth and hydrate film/shell growth at the water-hydrocarbon interface will be highlighted.

2.4.2.1 Single crystal growth

The hydrates can grow in different ways; one is the singles crystals growth in water-hydrocarbon solution. This type of growth occurs most often in states with low driving force conditions. For example, to investigate the effect of the additives on hydrate crystal growth and morphology, this is the most frequently experimental process used. Single hydrate crystals of tetrahydrofuran (THF, sII hydrate) and ethylene oxide (sI hydrate) can be easily made in the laboratory and isolated for structural analysis. Both chemicals are completely soluble in water and the hydrates can be formed at atmospheric pressure and at temperatures above the freezing point of water. In contrast, a single crystal of gas hydrates is much more difficult to produce and isolate and only a few studies have been able to obtain single crystals of gas hydrates for structural analysis (Sloan and Koh, 2008).

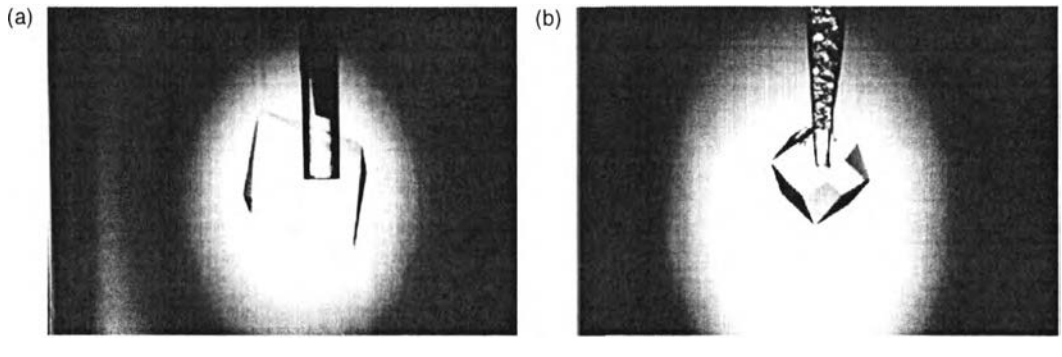

Figure 2.13 Photograph of single hydrate crystals of (a) tetrahydrofuran (sII); (b) ethylene oxide (sI) (Sloan and Koh, 2008).

Figures 2.13a and 2.13b shows the single hydrate crystals of structures I and II. As seen form Figure 2.13a, the structure II hydrate grown from the stoichiometric solution of THF. Figure 2.13b shows a structure I hydrate that is

grown from a stoichiometric solution of ethylene oxide in the resting conditions. These single crystals show exhibits (110) and (111) crystal planes of structure I and II, respectively. It should be noted that the single crystal growth is the slowest growing planes that are observable, while the fast growing planes are rapidly disappearing (Sloan and Koh, 2008).

From all the studies on this subject Smelik and King (1997) comes up with a hypothesis that the (111) planes in structure II are the slowest growing. This comes from the fact that it consists of the predominance of hexagonal face compared to the other crystal planes in sII. The reason that these crystal planes containing the predominance of hexagonal face grows slower than the others is because they is considerably more strained (120° between O-O-O angles) than those pentagonal faces (108°), with respect to either tetrahedral O-O-O angle (109°) or water angle (H-O-H of 104, 5°). Also the (110) plane of the sI crystal has a similar argument (Smelik and King, 1997).

2.4.2.2 Hydrate film/shell growth at the water hydrocarbon interface

The hydrate nucleation and growth is usually initiated at the water-hydrocarbon interface. The measurements of the growth of a hydrate film (or shell) at of the water-hydrocarbon interface provides insight into the growth mechanism which may be incorporated in realistic hydrate growth models (Sloan and Koh, 2008). Several studies about the hydrate film/shell growth at the water hydrocarbon interface show that the morphological are generally changed regardless of the same hydrate former. That is the saturation (or the driving force) has an effect on morphology, and there are similarities between growth behavior at a water-hydrate former planar interface and at the surface of a liquid droplet (Sloan and Koh, 2008).

Servio and Englezos (2003) studied the effect of the driving force pressure on the morphology of methane and carbon dioxide hydrates grown from droplets of water at 5 and 2.5 mm in diameter immersed in a hydrate-forming gas atmosphere. To prevent the water droplets wetting the surfaces, they were laid on a Teflon coated surface of stainless steel. In every experiment two or three droplets of water were used in the crystallizer tank. At the first five seconds after core formation at high driving force, the result could be seen. The surface of the droplet

appeared roughened and dull with many fine needle-like crystals extruding away from the gas hydrate-water interface, as seen in Figure 2.14. The same morphology is observed for methane and carbon dioxide hydrate former gases.

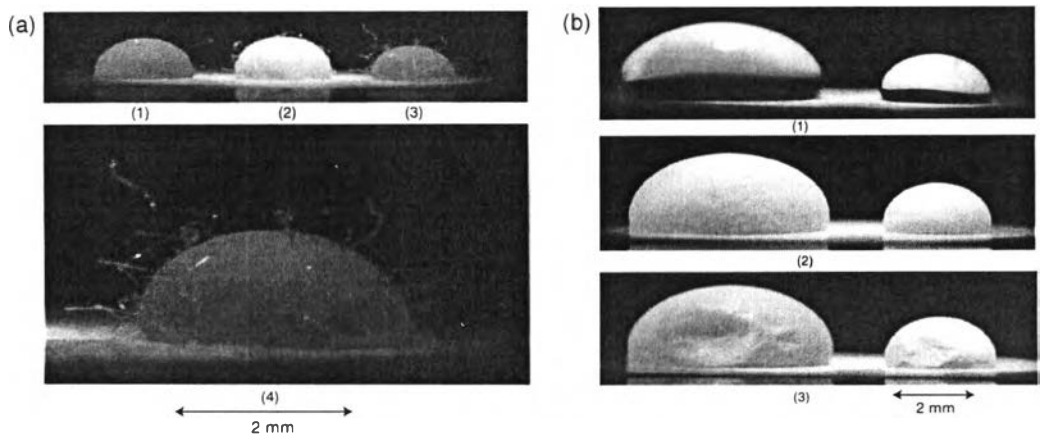

Figure 2.14 (a) Methane hydrate covering the surface of water droplets (1, 2, 3) under high driving force, 10 min after nucleation. Image (4) is a magnified view of droplet (3), and (b) methane hydrate covering two water droplets under low driving force at three different times: (1) at $t = 0$, (2) at $t = 10$ h where the water droplet is covered by hydrate, (3) at $t = 25$ h where the water droplet is covered by hydrate and depressions in the hydrate layer appear (Servio and Englezos, 2003).

Based on the experiments from Servio and Englezos (2003), they suggested that with high driving force applied on the system, the hydrate consists of three growth phases: 1) The appearance of a hydrate layer (shell) around the water droplet with needle-like crystals, and up to 10 h after nucleation the needle-like crystals grow in size and thickness, 2) The crystal needles collapse onto the hydrate layer covering the droplet, 3) The appearance of depressions in the hydrate layer surrounding the water droplet, which occurred within 10-15 h to a couple of days in some experiments. At high driving force pressure, it hardly controls where the hydrate will grow due to it can grow multiply in many different places. However, at low driving force the growth behavior was totally different; the hydrate is more predictable, in both grow and location.

The difference between high and low driving force pressure

can be seen in Figures 2.14a and 2.14b. As seen from the figure, a droplet at low driving force pressure (Figure 2.14b), there are no signs of hydrate crystals on the surface, while at high driving force pressure (Figure 2.14a), the hydrate crystal is observed. That is because the high driving force produces a greater number of core element areas compared to the low driving force. This is in agreement with Mullin (2001), who reported that the rate of nucleation depends on the number of nuclei formed per time per unit volume, which is increased with the degree of supersaturating. The supersaturating is proportional to the driving force meaning that that where there is high driving force is where the core of many sites are present. Therefore, the result is more random crystal growth and thus a rougher surface.

2.5 Hydrate Dissociation Process

Hydrate dissociation is a key importance in gas production from natural hydrate reservoirs and in pipeline plug remediation. it is an endothermic process, in which heat must be supplied externally to break the hydrogen bonds between water molecules and the van der Waals interaction forces between the gas guest molecules and water molecules of the hydrate lattice to decompose the hydrate to water and gas (Sloan and Koh, 2008). Although gas hydrates are known to occur in numerous marine and Arctic settings, little was known about the technology to produce gas from them. The proposed methods that can be used to dissociate a hydrate plug (in the pipeline) or hydrate core (in oceanic or permafrost deposits) are shown in Figure 2.15, including thermal stimulation, depressurization, and thermodynamic inhibitor injection, or a combination of these methods. The thermal stimulation and depressurization have been well quantified using laboratory measurements and state-of-the-art models (Sloan and Koh, 2008; Demirbas, 2010; Koh *et al.*, 2011).

Recently, several studies have shown that it may be possible to produce methane from hydrates by displacing the methane molecule in the hydrate structure with carbon dioxide, thus releasing methane and sequestering the carbon dioxide (Lee *et al.*, 2003; Graue *et al.*, 2006; Deusner *et al.*, 2012).

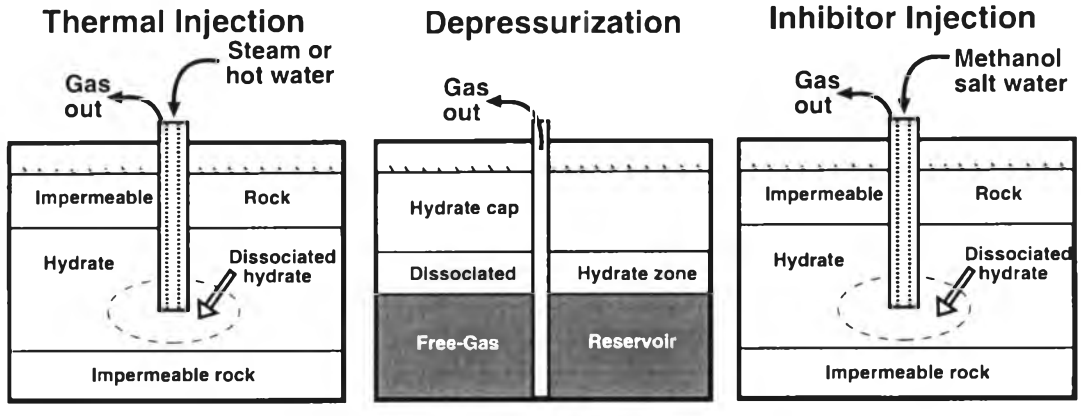

Figure 2.15 Schematic of proposed gas hydrate production techniques (Collett *et al.*, 2002).

Among the possible techniques for production of natural gas from in-situ gas hydrates, depressurization is considered to be the most economically promising (Collett, 2002). However, extraction of gas from a gas-hydrate accumulation by depressurization may be hampered by the formation of ice and/or the reformation of gas hydrate because of the endothermic cooling nature of gas-hydrate dissociation.

"Self-preservation" is the phenomenon, at which the hydrates can remain stable for extended periods outside the hydrate stable region as presented in Figure 2.16. The self-preservation or anomalous self-preservation has been experimentally observed by a numerous researchers (Stern *et al.*, 2001a, 2001b, and 2003; Takeya *et al.*, 2000; Giavarini and Maccioni, 2004; Kuhs *et al.*, 2004, 2005; Shimada *et al.*, 2005). However, little is understood of this phenomenon. The ability to increase and prolong the stability of gas hydrates is desirable for gas storage applications. As seen from Figure 2.16, the anomalous preservation region is observed over the temperature range 242–271 K on rapid depressurization to 0.1 MPa. This anomalous behavior has been also called "anomalous self-preservation." The latter consists of a short rapid dissociation phase with a release of 5–20 vol% of the total methane in the hydrate sample. During this gas release, adiabatic cooling of methane as well as general heat absorption occurs. After this rapid dissociation phase, the methane hydrate remains "metastably preserved" for up to 2–3 weeks depending on the

dissociation temperature (Stern *et al.*, 2003).

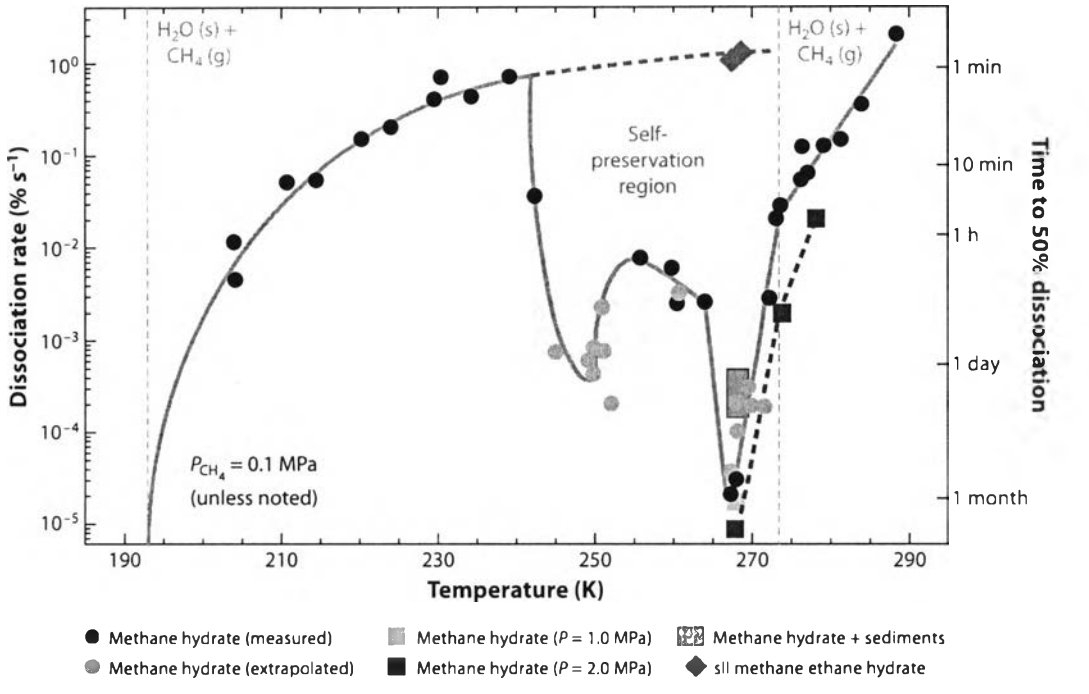

Figure 2.16 Self-preservation of hydrates (dissociation rate left ordinate, and time for 50% dissociation on right) as a function of temperature. The extrapolated times is shown as a dashed line versus the black points representing observations in the self-preservation region (Stern *et al.*, 2003; Koh *et al.*, 2011).

The cause of the anomalous "self-preservation" behavior is not well-understood. Stern *et al.* (2003) acknowledged that the ice-shielding could explain the self-preservation of residual gas hydrate (<8%) in temperature-ramping tests and in low-temperature rapid-depressurization tests. However, they suggested such an ice protection cannot adequately explain anomalous preservation of methane hydrate at 242–271 K, particularly as sII hydrate does not exhibit anomalous preservation. Kuhs *et al.* (2005) stated that, from neutron diffraction and SEM data, the anomalous "self-preservation" could be due to significant annealing of ice stacking faults (ice defects) at around 240 K. In addition, they suggested that below 240 K, the ice covering the hydrate has gaps between ice crystallites, which allow gas diffusion.

2.6 Hydrate Equilibrium Conditions

Gas hydrates are stable under low temperatures and high pressures. The hydrate stability zone in marine environments is a function of the water depth, the seafloor temperature, and the geothermal gradient. Any changes to the temperature or pressure, both at the surface and in the area adjacent to the hydrate, will affect the thickness of the stability zone. Although temperature and pressure are the main influencing factors in the formation of gas hydrates and the thickness of the hydrate stability zone, other factors, such as gas chemistry and gas availability, will also alter the thickness and location of the hydrate stability zone (Nixon and Grozic, 2006).

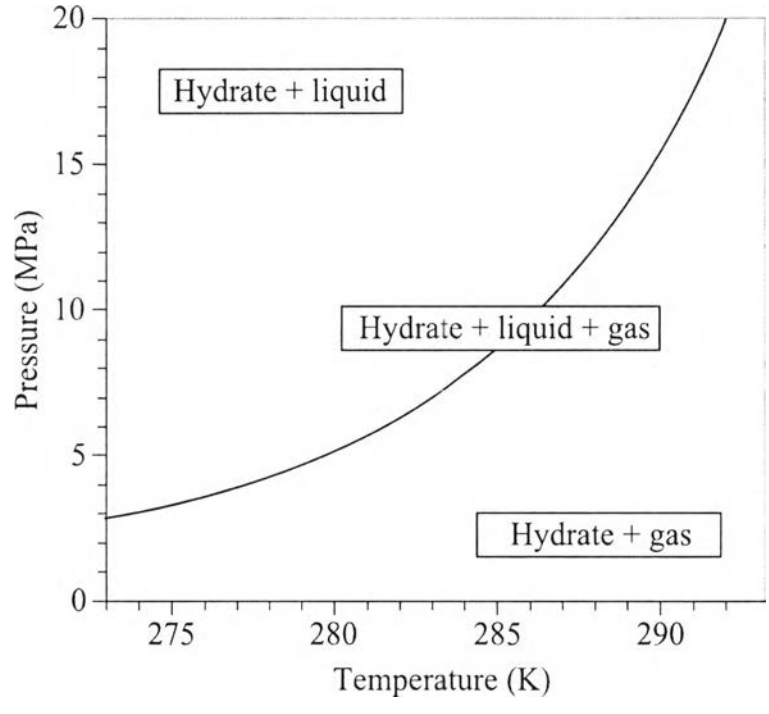

Figure 2.17 Phase equilibrium diagram for methane hydrates (Demirbas, 2010).

Figure 2.17 shows the phase equilibrium diagram for methane hydrates. At pressures and temperatures outside the hydrate stability zone, melting and decomposition of gas hydrates will occur. The hydrate decomposition will result in the release of water and methane gas, but requires input of heat. As decomposition occurs, the gas and water released cause a volume expansion. If the heat transport

and the pressure change processes are fast compared with the pore pressure dissipation processes, the excess pore pressure and the reduction in the effective stress can be estimated (Nixon and Grozic, 2006). The decomposition of gas hydrates can stem from any change in the pressure and temperature regime in the hydrate stability zone and results in a significant volume change. In addition, the distance from the equilibrium conditions is the driving force for hydrate formation. Hence, the hydrate equilibrium curve represents the pressure and temperature conditions where the hydrates dissociate.

2.7 Hydrate-based Technologies

The enormous reserve of methane gas in the hydrate state is considered as the future energy source. The global estimate of the methane hydrate resource is significantly larger than the estimate of global conventional natural gas resources (Milkov, 2004; Kvenvolden, 1999; US Geological Survey, 2000). Besides, the ability of gas hydrates to contain 150-180 volumes of gas/volume of hydrate makes them to be considered as a potential for natural gas storage and transport (Sun *et al.*, 2003). However, the practical exploitation of this opportunity requires the ability to preserve the hydrate in a predictable and controllable manner (Stern *et al.*, 2001b). Storage of CO_2 in natural gas hydrate reservoirs and at the same time releasing the hydrocarbon gas trapped in the hydrate state could be considered as double opportunities (Kvamme *et al.*, 2007). Thus, being fuel for the future and means of transporting and storing natural gases, gas hydrates are promising to alleviate problems related with these issues. In fact, getting the gas out of the natural hydrate state or storing the gas in a hydrate state is a challenge that has attracted many researchers. Gas storage and transportation based on hydrate technology has been a focus for many researchers (Gudmundsson and Brrehaug, 1996; Khokhar and Sloan, 1998; Zhong and Rogers, 2000; Gudmundsson *et al.*, 2002; Guo, *et al.*, 2002).

2.7.1 Separation of Gas Mixtures

When a gas mixture forms hydrate with water partially under certain conditions, the water-free concentration of each component in the hydrate phase and

that in the residual vapor phase will be different. The component that forms hydrate more easily will be enriched in the hydrate phase. Based on this principle, it is considered possible to separate gas mixtures through forming hydrate. Hydrate-based separation concepts have been proposed for many fields: (1) recovering global warming gases, such as hydrofluorocarbon from air, sulfur hexafluoride (SF6) from nitrogen, and CO_2 and H_2S from flue gas; (2) recovering organic contaminants from gaseous or aqueous mixtures; (3) recovering hydrogen from hydrogen-containing light hydrocarbon gas mixtures; (4) recovering methane from low-concentration coal mine methane; and (5) separation of methane and ethane, which is required in natural gas, oil processing, and ethylene production. The hydrate-based gas separation is more effective and has many advantages over conventional separation methods, such as cryogenic fractionation, selective adsorption, gas absorption, and membrane process (Sun *et al.*, 2011).

2.7.2 Carbon Dioxide Sequestration

Carbon sequestration is defined as the removal of greenhouse gases from industrial or utility plant streams and their long-term storage in such a way that they cannot interact with the climate system (Giavarini *et al.*, 2007). Carbon dioxide and water can form a stable hydrate when pressure and temperature fall within the hydrate formation region. For instance, injecting CO_2 into the deep-sea sediments, it resides in the liquid phase and gravitational stable. In addition, CO_2 hydrate formation will impede the flow of liquid CO_2 (Giavarini *et al.*, 2007; House *et al.*, 2006). Since CO_2-containing hydrates are considerably more stable thermodynamically than methane hydrates, it is a possible way to replace the original hydrate bound hydrocarbons by CO_2 (Giavarini *et al.*, 2007). Two goals can be accomplished at the same time: safe storage of carbon dioxide in the hydrate reservoirs, and in situ release of hydrocarbon gas. The hydrate and the matrix mineral surfaces are separated by liquid-containing channels, which will serve as escape routes for released natural gas, as well as distribution channels for injected CO_2 (Kvamme *et al.*, 2007).

2.7.3 Natural Gas Storage

According to the highly concentrated gas in the hydrate form, for example, 1 m^3 of methane hydrate contained 170 m^3 of methane gas at STP (Sun *et al.*, 2003; Englezos and Lee, 2005). The storage of natural gas is appealing for industrial utilization because of not only its high storage capacity, but also its high safety. Gas hydrate can be stored at 15 °C under atmospheric pressure for 15 days, retaining almost all the gas (Gudmundsson *et al.*, 1994). Methane hydrate remains metastable at 0.1 MPa and temperatures slightly below 0 °C for a certain of time (Stern *et al.*, 2001a). The preservation is improved if the pressure is kept at 0.2 or 0.3 MPa and depends on the concentration of methane gas molecules in the hydrate (Giavarini and Maccioni, 2004). The anomalous preservation has potential applications for successful retrieval of natural gas hydrate or hydrate-bearing sediments from remote settings, as well as for temporary low-pressure transport and storage of natural gas (Stern *et al.*, 2001a). A confocal scanning microscope is used to explain the anomalous preservation behavior of CH_4 hydrate (Shimada *et al.*, 2005). That is the increase in storage stability of CH_4 hydrate above 240 K is likely related to the formation of the ice. With high energy density, gas hydrate can be used in storage and transportation of natural gas, which has certain advantages over highly compressed or liquefied gas at higher temperatures and lower pressures. Particularly, for a medium- or small-scale natural gas field, where it is not appropriate to use liquefied natural gas or pipeline transportation, natural gas hydrate is a more economical solution (Sun *et al.*, 2011).

However, industrial applications of hydrate storage processes are hindered by some problems, such as slow formation rates, unreacted interstitial water as a large percentage of the hydrate mass, reliability of hydrate storage capacity, and economy of process scale-up (Mandal and Laik, 2008). Due to the solubility of natural gas in water is very low, only a thin hydrate film is formed at the interface between the water and gas without stirring or other enhancing measures. To solve these problems, two approaches including mechanical and chemical means are generally adopted, which are similar to those methods used in hydrate-based gas separation processes. The mechanical method includes stirring (Iwasaki *et al.*, 2005; Takaoki *et al.*, 2005), spraying of liquid in continuous gas phase (Fukumoto *et al.*,

2001; Ohmura *et al.*, 2002), bubbling of gas in continuous liquid phase (Luo *et al.*, 2007), microbubbling (Takahashi *et al.*, 2002), and icing (Stern *et al.*, 1996). Gas hydrate can also be shaped into pellets using mechanical method, and treated as a slurry medium with some cooling medium or type of oil. The pelletized natural gas hydrate is expected to be able to improve the transportation and storage efficiency, self-preservation effect, and handling efficiency (Takaoki *et al.*, 2002; Rehder *et al.*, 2012).

In comparison with other natural gas storage and transportation methods, such as liquefied transportation, a substantial cost saving (18% - 24%) is expected for the transport of natural gas in the hydrates form (Gudmundsson *et al.*, 2002; Javanmardi *et al.*, 2005). For distant markets, the most popular method of transporting the natural gas is liquefied natural gas (LNG). This technology requires expensive capital investment and so is suitable for huge gas reserves. The natural gas hydrate (NGH) method avoids the capital cost investment for the infrastructure constructions of the LNG method, which is an important point for the transportation of stranded gas. Therefore, especially for the stranded gas, the NGH method can be considered as an alternative for transportation of natural gas (Nakayama *et al.*, 2010).

To store gas in the form of hydrate, the crucial issues such as slow formation rates, unreacted interstitial water as a large percentage of the hydrate mass, reliability of hydrate storage capacity, hydrate stability must be improved. There are many researchers studied and investigated on gas hydrate formation and dissociation by using hydrate promoter including chemical promoters and porous mediums.

2.8 Hydrate Promoters

One of the drawbacks for the development of hydrate-based processes is due to the high-pressure requirement of such systems, which makes the processes less feasible and economically less attractive. To overcome this specific problem, additives or promoters are commonly introduced to clathrate hydrate systems in order to dramatically reduce the equilibrium pressure and to make hydrate technology economically more attractive.

2.8.1 Sodium Dodecyl Sulfate (SDS)

The key effect of surfactant is that it reduces the gas-liquid interface surface tension, so that the diffusion resistance between two phases is reduced and the gas molecules solubility is increased, as a consequence, better mass transfer effects is gained. However, the promotion mechanism of surfactants is not very clear yet.

Zhong and Rogers (2000) investigated the effects of sodium dodecyl sulfate (SDS) surfactant on ethane hydrate formation in the quiescent system. The result showed that the hydrate formation rate was increased with the presence of SDS in a quiescent system. They revealed that a critical micelle concentration (CMC) of SDS solution was found to be 242 ppm at the hydrate formation conditions, where CMC was the best determined by hydrate induction time. The interesting result was the adsorption of hydrate-surfactant particles on the metal surface that prevented the gas to form the hydrate further in free water. The solution level in the sample cell was then decreased as the hydrate particles were removed from the bulk water and attached to the stainless steel wall. As a result, they noted that the results from their experiment have positive implications for large-scale utilization of the unique gas storage properties of gas hydrates.

Karaaslan and Parlaktuna (2000) studied the effects of different types of surfactants (cationic, anionic, and non-ionic) with the concentration range of 0.005 – 1 % by weight on methane hydrate formation kinetics at temperature range of 17.6 – 19.0 °C and pressure range of 574 – 578 psig in a stirred reactor at 500 rpm for all experiments. They indicated that there was no effect of surfactants on the thermodynamics of the hydrate formation. An anionic surfactant showed the best gas hydrate promoter by increasing the hydrate formation rate for all concentrations. In addition, cationic surfactant was effective as a promoter at low concentration, while non-ionic surfactant was less pronounced.

Ganji *et al.* (2007b) also investigated the effects of different surfactants on methane hydrate formation rate and storage capacity. Anionic surfactants–sodium dodecyl sulfate (SDS) and linear alkyl benzene sulfonate (LABS), cationic surfactant–cetyl trimethyl ammonium bromide (CTAB), and non-ionic surfactant–ethoxylated nonylphenol (ENP) were used. The experiment was

conducted by pressurizing with methane gas up to 8.3 MPa at 298.2 K. After reaching the equilibrium at initial temperature and pressure, the system was then cooled to the hydrate formation temperature at 276.2 K with the agitated system of 200 rpm. They stated that the key function of methane hydrate-promoting agent was to improve the solubility of the hydrate forming gas in water. The results showed that the methane hydrate formation rate was increased with the presence of surfactants in all cases compared to pure water. In addition, for all hydrate samples at each constant temperature, the maximum dissociation rate occurred at the beginning of dissociation stages and then the rate decreased. This result may be the phenomenon called the self-preservation, which an ice layer was formed around hydrate crystals during hydrate dissociation that prevented the hydrate from further dissociation. As a result, they indicated that among the surfactants tested, SDS was the best one for utilizing methane hydrates for storage and transportation of gas with the maximum promotion effect on hydrate dissociation rate while the stability of hydrate formed was satisfactory at 268.2 K.

In 2008, the effects of sodium dodecyl sulfate (SDS) on ethane hydrate formation and dissociation were reported by Mandal and Laik (2008). They conducted the experiment at 255 K in the quiescent system. It can be observed that in the presence of SDS, ethane hydrates grew as fine particles, which increased the gas consumption and the storage capacities. Moreover, the addition of SDS in the ethane-water system changed the energy of the intermolecular interaction and the equilibrium between water and gas. Therefore, SDS showed the thermodynamic effect on ethane hydrate formation, caused in a shift of formation temperature. The hydrate dissociation rate was also investigated. The results showed that in the presence of SDS increased the hydrate dissociation rate due to the low self-preservation effect. The picture of ethane hydrate in their study is shown in Figure 2.18.

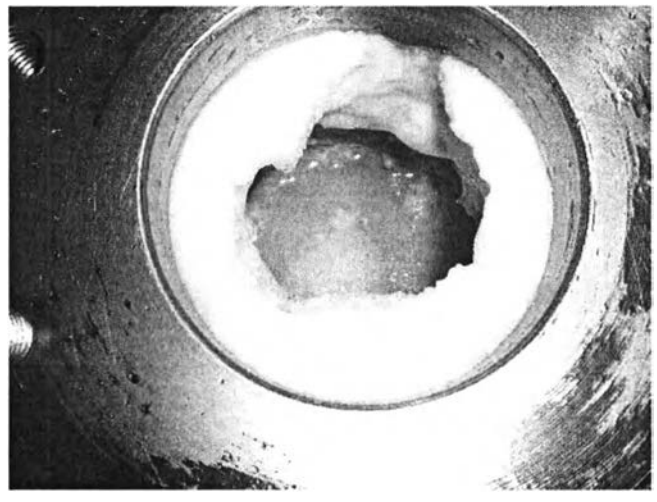

Figure 2.18 Picture of ethane hydrate cluster in an opened reactor (Mandal and Laik, 2008).

Yoslim *et al.* (2008) studied the effect of anionic surfactant on morphology of methane/propane hydrate crystal. The experiment was performed by using sodium dodecyl sulfate (SDS) with concentrations of 645 and 2,200 ppm (below the CMC) at temperature and pressure range of 2.4 – 5.3 °C and 1,430-3,200 kPa, respectively, in the agitated system. They found that the hydrate formation took place at the gas-liquid-solid line, the sidewall or tip of a thermocouple. On the other hand, in the absence of SDS, the hydrates appeared as a thin film at the gas-liquid interface. The branches of fibre-like crystals were observed when the surfactant was added in the system. In addition, the addition of surfactant decreased the surface tension of liquid water resulting in the creation of a film-like interface along the wall and below the gas-liquid-solid line. They believed that this film was preferred location for nucleation and initiation of hydrate growth. Moreover, The degree of fibre-like branching was found to increase with the increasing of surfactant concentration and at the higher degree of undercooling caused the faster of hydrate growth.

Jiang *et al.* (2008) studied the effect of SDS and tetrahydrofuran (THF) on methane hydrate formation. The experiment conducted using 0.04 wt% of SDS solution and mixed 0.04 wt% of SDS and 0.04 wt% of THF solution in a quiescent condition. The results were in agreement with the previous literature

works, which showed that the presence of SDS surfactant can help to form the hydrate rapidly in the static system. Mixed SDS-THF solution showed a higher hydrate formation rate than that with only SDS solution. They implied that, with the presence of SDS, there was the hydrate massive on the wall of reactor during the hydrate formation process resulting in the rapid hydrate formation, while the effect of THF cannot be rationally explained at that time.

In 2013, Partoon *et al.* investigated the potential of sodium dodecyl sulfate (SDS) as low-dosage promoter for carbon dioxide hydrate formation. The experiments were conducted by using a various SDS concentrations up to 3,000 ppm at temperature of 273.65 K and 35 bar. The results indicated that the induction time decreased with the increase of initial carbon dioxide pressure due to the increase of driving force pressure in the system. The addition of SDS reduced the induction time and significantly increased the carbon dioxide uptake. Furthermore, they stated that the addition of SDS solution with concentration of 700 ppm increased the carbon dioxide consumption eight times more than the system without any addition of SDS solution. This result was attributed to the SDS kinetic promotion effectiveness. At this concentration, more gas can be captured by water molecules and the amount of gases encapsulated by hydrate will increase. However, they noted that after capturing a certain amount of gas, no more hydrate could be formed due to the thermodynamic limitation or full occupation of cavities. In addition, at higher concentration, the amount of carbon dioxide consumption reduced with the increase of SDS concentration, which was attributed to the formation of micelles in the system by SDS and the anti-agglomerating effects of SDS on gas hydrate. Moreover, they showed that with a low dosage of SDS, the carbon dioxide consumption increased tremendously, which was important for the development of gas hydrate-based processes.

Sun *et al.* (2013) studied the effects of surfactants and liquid hydrocarbon on gas hydrate formation rate and storage capacity. The experiments of hydrate formation were carried out in the pressure range of 3.69 - 6.82 MPa and the temperature range of 274.05 - 277.55 K with a stirrer. Surfactants, sodium dodecyl sulfate (SDS) and dodecyl polysaccharide glycoside (DPG), and liquid hydrocarbons, cyclopentane (CP) and methylcyclohexane (MCH), were used in the experiment. The

results showed that gas hydrate could form at higher hydrate formation rate in a quiescent system with the presence of surfactant compared to the hydrate formation in a stirred pure water system. Moreover, the highest storage capacity was observed in SDS solution at 274.05 K and 5.54 MPa at 163 V/V, while the storage capacity in DPG solution was lower than that in SDS solution at all cases. In addition, the effect of the mixtures of surfactant (SDS or SDS+DPG) and cyclopentane on hydrate formation rate was more pronounced compared to surfactant (SDS or SDS+DPG) only, but the gas storage capacity in hydrates had a little drop with the presence of cyclopentane.

Kumar *et al.* (2013) studied the influence of contact medium and surfactants on carbon dioxide hydrate kinetics at experimental condition of 274 K and 3.55 MPa in the quiescent system. Three different surfactants were used in the study, Tween-80 (non-ionic surfactant), dodecyltrimethylammonium chloride (DTACI) (cationic surfactant), and sodium dodecyl sulfate (SDS) (anionic surfactant). In addition, silica gel with particle size of 230-400 mesh was used in all experiments, which was saturated by surfactant solution before conducting the experiment. The results clearly showed that the induction time of carbon dioxide hydrate reduced upon increasing the SDS concentration. For non-ionic surfactant, the rate of hydrate formation was not improved when increasing the concentration due to the hydrate particles separated from each other; however, at the end of experiment at 10 h, the total moles of gas consumed had no significant difference for all concentrations. For cationic surfactant, the lowest gas consumption rate was observed compared to the other two surfactants because of particle aggregation, which blocked mass transfer through the solid hydrate, and the cationic surfactant (DTACI) was defined as the hydrate formation inhibitor. For anionic surfactant, the gas consumption after 30 min of hydrate formation was almost twice compared to the other two surfactants at high concentration; however, at lower SDS concentration, no significant difference was observed both in the initial rate of hydrate formation and the final gas consumption. They suggested that anionic surfactant considerably enhanced the rate of gas uptake in the presence of silica gel, and it can be used as a kinetic promoter of gas hydrate.

Hao *et al.* (2014) used sodium dodecyl sulfate and coal to enhance

methane hydrate storage capacity at temperature of 273.15 K and pressure of 4 and 6 MPa. The SDS solution of 300 mg/L was used in their experiment. For the material preparation, coal was soaked in distilled water and SDS solution before conducting the hydrate formation experiment. The results showed that the maximum methane storage in the hydrate form were 160.54 V/V and 179.97 V/V at 4 and 6 MPa, respectively, in coal, which was saturated by SDS solution. This result confirmed the effect of SDS that played a critical role to accelerate the hydrate-forming process in coal. In addition, the rate of hydrate formation was improved up to 58.26 cm^3/min. They concluded that all enhancements convinced the feasibility for a cost-effective methane gas storage application at large scale.

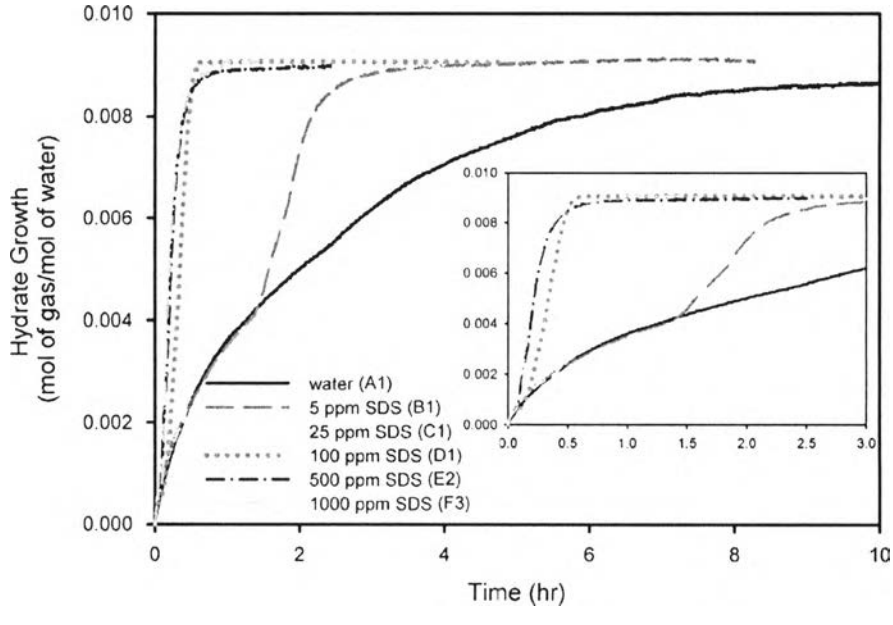

Figure 2.19 Two-stage of hydrate growth profiles influenced by surfactant at various concentrations of mixed hydrogen/propane (90.5/9.5 mol%) gas mixture (Veluswamy *et al.*, 2015).

Currently, anionic surfactant (SDS) was also used to enhance the kinetics of mixed hydrogen/propane hydrate formation (Veluswamy *et al.*, 2015). The concentrations of SDS were prepared at 5, 25, 100, 500, and 1,000 ppm. The experiments were conducted at constant pressure and temperature of 8.5 MPa and 274.2 K, respectively, in the agitation system. The result indicated the stochastic

nature of hydrate nucleation. Moreover, they stated that SDS surfactant played a significant role to improve the kinetics of mixed hydrogen/propane hydrate formation. On the other hand, the rate of mixed hydrogen/propane hydrate formation was improved with the presence of SDS surfactant, even low concentration. Higher concentrations of SDS (100 ppm and 500 ppm) were found to be very effective in promoting the formation of mixed hydrate with completion of experiment in approximately 30 min from the nucleation point, while the control system (pure water) took a longer time at about 10 h. They observed the deflection point, which was the curve of gas uptake deflected from the control system (pure water) and the time at which the deflection occurs, called deflection time. They noted that the two-stage of hydrate growth was observed when SDS was added. The first stage represented water-like behavior (without any surfactant), related to the slow rate of hydrate formation. The second stage that followed after the deflection point was characterized by a faster rate of hydrate formation due to the hydrate growth promoting effect, exhibited by the presence of SDS surfactant as shown in Figure 2.19. Furthermore, they proved that the SDS surfactant acted as kinetic promoter only without altering the thermodynamic of hydrogen/propane/water system due to the final gas uptake achieved was similar in all tested concentration of SDS solution and for pure water.

2.8.2 Tetrahydrofuran (THF)

THF is the chemical hydrate promoter, which remarkably reduces the required hydrate formation pressure and increase the required temperature to form gas hydrates due to its effect on the thermodynamics equilibrium of gas hydrates.

Florusse *et al.* (2004) studied the hydrogen cluster stored in a binary THF-H_2 clathrate hydrate at low pressure. They demonstrated that the stability region of binary THF-H_2 clathrate hydrates extended to relatively low pressures at temperatures closed to the ambient (~15 MPa at 10 °C). Powder X-ray diffraction confirmed clathrate to be of structure II (sII) and the large hexakaidecahedral ($5^{12}6^4$) cavities were fully occupied by THF, observed by using Raman and magic-angle spinning (MAS) NMR with up to one H_2 molecule per small dodecahedral cage. While the relatively low-pressure stability of this binary clathrate hydrate was

promising with respect to the hydrogen storage, THF occupied the large cavities that might accommodate hydrogen, meaning that the stability was increased at the sacrifice of H_2 content; one hydrogen molecule per small cage equals only 1 mass % H_2. This result indicated that the large cavities of structure II hydrate were partially occupied by hydrogen. They concluded that THF promoter guest molecules could be used to store hydrogen in a binary clathrate hydrate at low pressure. Therefore, optimizing the promoter system might increase the storage capacities.

Lee *et al.* (2005) studied the mole fraction of tetrahydrofuran (THF) for tuning the clathrate hydrates for hydrogen storage. Firstly, THF hydrate was formed below the melting point at 277.3 K. The THF hydrate was then pressurized with hydrogen gas at various pressure up to 120 bar. For the initial result, they found that the full loading of small cavities of structure I (sI) of THF hydrate with hydrogen would be 2.1 wt% of H_2. In order to increase the hydrogen content of the hydrate, the hydrogen guest must enter the large cavities of structure II (sII). The interesting result was that at 1.0 mol% and down to 0.15 mol% of THF, the mole ratio of H_2/THF increased above 4 to as high as 23 for the 0.15 mol%. It indicated that the large cages must contain hydrogen. They noted that 1.0 mol% of THF was approximated at the eutectic composition of THF hydrate. However, at lower THF concentration, 0.1 mol%, a hydrogen-containing hydrate was no longer formed. They explained that the combination of hydrogen pressure and THF concentration was insufficient to fill the large cages in the structure to produce the stable hydrate. In addition, they stated that it was possible to introduce the other gas guest molecules such as methane into the large cages of structure II hydrate.

In 2006, Strobel *et al.* investigated the molecular hydrogen storage in binary THF-H_2 hydrates. THF solution was prepared at concentration range of 0.5 - 5.56 mol%. For experimental method, THF hydrate was firstly formed in a freezer at temperature approximately 250 K for 3 days. Then THF hydrate was crushed under liquid nitrogen and sieved to the desired particle size (<45 or <250 μm). The crushed THF hydrate was loaded to the cell for conducting the binary THF-H_2 hydrates, which was pressurized by hydrogen gas up to 13.8 MPa. The temperature was cycled between 270 and 278 K every 8-12 h for 7 days for stoichiometric experiment and 265 and 270 K for nonstoichiometric. The result showed that the hydrogen storage

increased asymptotically to 1.0 wt% when the initial formation pressure was increased. This storage corresponded to the storage capacity of stoichiometric binary THF-H_2 hydrates with one hydrogen molecule per small cavity presented in this study. Moreover, they strongly confirmed that THF remained the favorable guest for the hydrate in the large cage ($5^{12}6^4$) due to the hydrogen storage capacity was not changed when the concentration was decreased from 5.56 mol% to 0.5 mol% at constant pressure of 13.8 MPa.

The controversy over the binary THF-H_2 hydrate content is resolved by Anderson *et al.* (2007). They demonstrated the phase relation and binary clathrate hydrate formation in the system of THF-H_2-H_2O. The result confirmed the formation of structure II binary THF-H_2 hydrate with stoichiometric THF-to-water ratio of 1:17. Some parts of the experiment was followed Lee *et al.* (2005) that decreased the THF concentration from 5.56 mol% to 0.2 mol%, which was lower than the eutectic composition of THF hydrate (1 mol%). The result indicated that at lower THF concentration (0.2 mol%), the stoichiometric THF:water was the same as 5.56 mol% of THF at 1:17. They strongly confirmed that at the low concentration of THF (below 1.0 mol%), the hydrogen gas did not occupy in the large cages of structure II, and only THF was formed the hydrate in this occupancy.

Giavarini *et al.* (2008) investigated the mixed THF-CH_4 hydrates formation and dissociation for methane storage. The mixed THF-CH_4 hydrates were formed by using an aqueous solution containing 19% by weight of THF, corresponding to the stoichiometric molar ratio (H_2O/THF = 17). The reactor, filled with THF solution was pressurized to 4.5 – 4.8 MPa with methane gas. The temperature was then lowered to 1 – 2 °C. They demonstrated that for the mixed hydrate formation, a conversion was calculated at about 30%, lower than that in the simple CH_4 hydrate. For the hydrate dissociation test, the results showed that the dissociation rate was lower with the increasing in storing pressure. On the other hand, the dissociation rate was higher when increasing the storing temperature. As a result for methane storage application, they noted that the best preservation conditions are realized at -1 °C and 3 MPa, which was required at about 66 days to complete the dissociation, against 16 days for methane hydrates.

The phase equilibrium of THF-CH_4 hydrates was demonstrated by

Mohammadi and Richon (2009). The equilibrium data was obtained from the hydrate dissociation experiment by using an isochoric pressure-search method. The experimental data was compared to the one reported in literature and showed an acceptable agreement that confirmed the reliability of the isochoric pressure-search method used in this work. Moreover, it was shown that the presence of THF in the aqueous solutions shifted the hydrate dissociation conditions of methane to high temperatures.

Prasad *et al.* (2009) observed the mixed THF-CH_4 hydrates by using Micro-raman spectroscopy. Mixed gas hydrates were synthesized with different THF concentrations from 1.46 to 5.88 mol% under the methane atmosphere. The result indicated that THF molecules occupied the large cages of sII hydrate in all cases. They stated that the formation of sII hydrates was occupied the unfilled cages (small cages) by CH_4 for THF concentration ranging from 2.95 to 5.88 mol%. At the same time, the Raman spectral indicated that mixed gas hydrates at 1.46 mol% of THF was non-uniform and the hydrate structure transformed from sII to sI due to the hydrate melting.

Chari *et al.* (2012) investigated the effects of low mole fractions of THF and *tert*-butylamine (*t*-$BuNH_2$) on phase stability of methane hydrate. The mole fraction of THF used in this study was 0.033, 0.0056 and 0.06. The results showed that, at 0.06 mole fraction of THF or *t*-$BuNH_2$, the mixed hydrate was observed only in structure II, and, at the mole fraction higher than 0.056, it had no effect on the phase boundary. Meanwhile, at the low concentration (low mole fraction), the phase boundary was shifted toward sI hydrate. In addition, the preferred structure of mixed hydrates was complex and co-existing of sI and sII at much lower concentration of THF. They observed the hydrate formation in two stages by interpreting from the *P-T* trajectory curve. The hydrates in the first stage (T=295 K) were mostly in sII, and in the second stage (T=275 K) were with sI structure. Furthermore, the hydrate dissociation profiles, formed in second stage, were significant difference from pure methane hydrates. They noted that the two liquid hydrocarbons, THF and *t*-$BuNH_2$, were considered as hydrate promoter for sI hydrates at low dosage.

Lee *et al.* (2012) studied the phase equilibrium of THF-CH_4, THF-CO_2, CH_4-CO_2, and THF-CH_4-CO_2 hydrates. The synchrotron X-ray diffraction

(XRD) and Raman spectroscopy were used to determine the structure and composition of the hydrates. From the experimental data, the dissociation boundary of THF-CH_4 and THF-CO_2 hydrates was shifted to lower pressures and higher temperatures from those of pure CH_4 and pure CO_2 hydrates. From the XRD measurements, they confirmed that the CH_4-CO_2 hydrate, which was prepared from the CH_4/CO_2 (50:50) gas mixture revealed the sI hydrate, whereas the THF-CH_4-CO_2 hydrate formed the sII hydrate. The Raman measurements of the CH_4-CO_2 hydrate indicated that the population of CH_4 molecules in the small 5^{12} cages of the sI hydrate framework was higher than that in the large $5^{12}6^2$ cages, while the CO_2 molecules preferentially occupied the large $5^{12}6^2$ cages. In the case of THF-CH_4-CO_2 hydrate, the CH_4 and CO_2 molecules were encaged only in the small 5^{12} cages of the sII hydrate framework, whereas the large $5^{12}6^4$ cages were fully occupied by THF molecules at the stoichiometric concentration of 5.56 mol %. The comparison of dissociation pressure of THF-CH_4 and THF-CO_2 hydrates with the THF concentration of 5.56 mol% is shown in Figure 2.20.

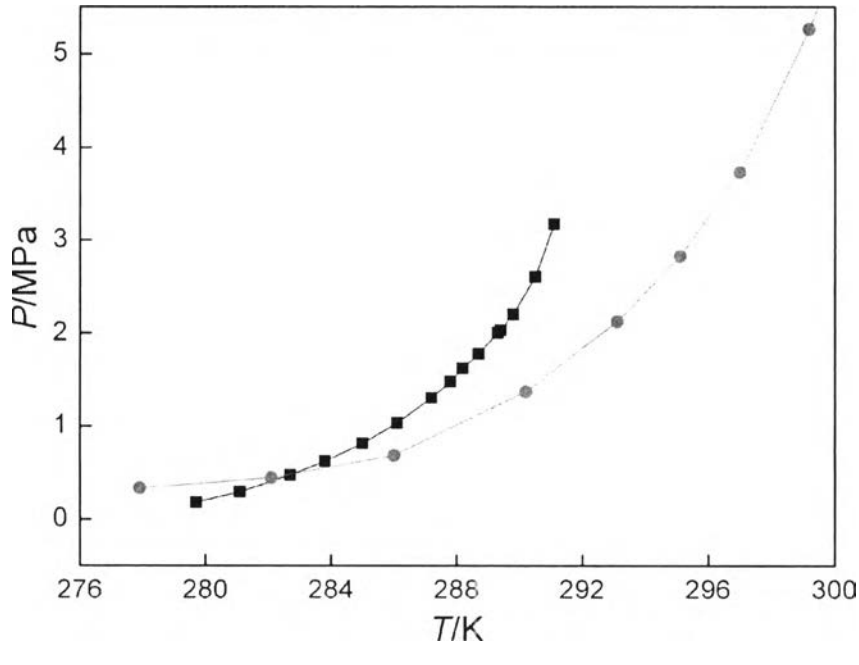

Figure 2.20 Comparison of dissociation pressure of THF-CH_4 (●) and THF-CO_2 (■) hydrates with the THF concentration of 5.56 mol% (Lee *et al.*, 2012).

Sharma *et al.* (2014) reported the formation kinetics of methane hydrate in aqueous solution of THF at concentration of 6.03 mol% and different pressures of the range 0.88 – 8.21 MPa in a stirred reactor. There was 90% of methane consumption for the hydrate formation in THF/CH_4/water system occurred significantly faster than CH_4/water system. It was observed that the increasing of initial pressure decreased the induction time of mixed THF-CH_4 hydrates. The overall hydrate yield in mixed hydrates—the small cages and large cages of sII were occupied by methane and THF molecules, respectively— was always more than pure methane hydrate in structure I. In addition, the significant amount of methane release occurred from mixed hydrate at temperature higher than the ice melting temperature. They noted that the mixed hydrates system could be used as medium to store and transport the methane gas.

In 2013, Veluswamy and Linga studied the kinetics of mixed THF-H_2 hydrates formation for hydrogen storage in a stirred tank reactor. THF concentration was varied between 1 mol% and 5 mol%. The results clearly demonstrated that, in the dissolution phase, the increase in the driving force pressure resulted in an increase in gas uptake until saturation for all concentrations of THF promoter. Moreover, the increase in concentrations of THF from 2.4 mol% to 5 mol% resulted in decreasing gas uptake. However, the increase driving force had a little effect on the reduction of induction time even at high promoter (THF) concentration. In addition, for any THF concentration, the rate of hydrate formation increased with the increase in driving force pressure. Hydrate growth increased with the increase in driving force for hydrogen/THF hydrates at all THF concentrations. Moreover, they also stated that faster induction times, higher rate of hydrate formation and higher gas consumption were desirable for a successful demonstration of the clathrate process for hydrogen storage.

After that, they investigated the impact of tetrahydrofuran (THF), tetra-n-butylammonium bromide (TBAB), and cyclopentane (CP) on clathrate hydrates of for hydrogen storage (Veluswamy *et al.*, 2014a). The experiments were conducted in the stirred reactor at the same pressure and temperature of 12 MPa and 279.2 K. The results showed that the highest hydrogen storage capacity was observed in THF/Hydrogen hydrate system. The hydrogen uptake of 0.0173 mole of gas/mole

of water (0.169 wt%H_2) was obtained for the 3.5 mol% THF solution and it was about 2 times higher than hydrogen uptake obtained for 3.5 mol% TBAB solution under the same conditions, while CP promoter did not nucleated the hydrate even at a very high driving force; however, only small amount of gas dissolution (0.0021-0.0025 mole of gas/mole of water) was observed. For the dissociation experiment, TBAB/Hydrogen mixed semi-clathrates took longer time to dissociate compared to THF/Hydrogen hydrates under the similar decomposition conditions. In addition, at the different concentration of promoters, a lower concentration led to increase the rate of hydrate dissociation.

Ricaurte *et al.* (2015) injected THF to trigger gas hydrate crystallization for the kinetic hydrate promoter application. Their method consisted of an in situ injection of small amount of THF into the liquid phase, contained of various concentrations of SDS, at pressure of 4 MPa and temperature of 275 K inside the hydrates metastable zone. They claimed that the stochastic behavior of methane hydrate formation was canceled out according to study the effect of SDS at any concentration by injecting THF into the system. The results also indicated that the higher the concentration of THF, the higher the hydrate formation rate regardless of the initial present of THF or injected. However, the intrinsic effect of SDS on hydrate formation kinetics would be accurately evaluated only if the quantity of THF injected was very small.

2.8.3 Porous Media

In 1988, Cha *et al.* added the third-surface (clay) to investigate its effect on natural gas hydrate formation. Bentonite (sodium montmorillonite) was selected for this study. The results showed that the pressure drop with the third surface was higher than that with pure water during the hydrate formation, indicating the gas had been encapsulated into the hydrates. They proposed that two important results were possible on the hydrate formation tests with the third surface. First, the thermodynamic promotion could be caused by the ordered adsorption of water molecules onto some surfaces as a structure that approximates a part of a hydrate lattice, and this surface becomes part of the hydrate structure. Second, the kinetic promotion could be influenced by the presence of an external surface, which

provides the nucleation sites. They summarized that the difference between the mechanism for kinetic promotion and thermodynamic promotion was that the former requires only that a surface adsorb water molecules into random clusters, which can encourage the formation of hydrate crystal leading to faster and greater crystal growth. However, the thermodynamic promotion requires that the surface to adsorb water molecules into ordered layers, which were close in structure to that of potential hydrate cages.

Riestenberg *et al.* (2003) studied the sediment surface effects on methane hydrate formation and dissociation. The colloidal suspensions containing bentonite were used in thier study. The operating condition of methane hydrate formation was 3 MPa and 5 °C, while the dissociation experiments were conducted by increasing the temperature or thermal stimulation technique. The result showed that the presence of bentonite decreased the overpressure, which was necessary for the onset of hydrate formation even at relatively low concentration. The hydrate dissociation experiments presented the distinct plateau in the temperature within the hydrate zone, indicating the hydrate dissociation behavior. In addition, the duration of distinct plateau was different at all experiments due to a consequence of the large thermal mass of the reactor vessel. They concluded that for natural gas hydrate deposits that consisted of mostly pure methane, stability may be little affected by sediment surface chemistries; however, it may significantly decreased the overpressure required for hydrate formation.

Yan *et al.* (2005) investigated the hydrate formation in wet activated carbon. The result showed that immersing activated carbon in water could enhance the formation of methane hydrate. The induction time period of 15 to 30 min, depended on the system temperature and initial pressure, was required for hydrate to form in fresh wet carbon. They also indicated that the pressure drop from the adsorption of wet carbon to methane was very small and can be negligible. The storage capacity of methane hydrate strongly depended not only on temperature and pressure but also on the mass ratio of water to carbon the size of activated carbon. In other words, the methane storage capacity increased with the increasing of initial pressure when temperature was fixed. For the effect of temperature, the storage capacity increased with the increase of temperature in high pressure range (~6-8.8

MPa), while it decreased in the low pressure range. They suggested that the most suitable condition for methane to from the hydrate in wet carbon was at ~278.0 K and ~8.0 MPa.

Klapproth *et al.* (2006) investigated the microstructure of methane hydrate in porous media, consisting of quartz, quartz + kaolite, and quartz + montmorillonite, at 10 MPa and 3 °C. The results on kinetics of methane hydrate formation indicated that the hydrate formation was initially fast due to the fast surface reaction with free water and gas access, and then slow down because the transformation of water into gas hydrate was limited by the gas and water transfer. In the system of quartz + kaonite, the gas consumption was much higher than quartz + montmorillonite system. They noted that dried montmorillonite could take up a part of water and protest it from the gas. However, the different reaction kinetics in the two systems (clay-containing sediments) reflected the different surface activities of mineral contents in the combination with free water or interfacial water. They concluded that the methane hydrates appeared between the quartz grains like cement. Kaolinite particles were observed as a filigree network on the surface of hydrate cement, while montmorillonite looked like flakes or crust. In addition, each of the minerals, used in a specific media composition, may play individual interaction with water and gas hydrate. The dissimilar kinetic features, using different porous media at the investigated conditions, led to confirm that porous media directly function on gas hydrate formation.

In 2009, Linga *et al.* investigated the effect of vessel size on gas hydrate formation with fixed bed silica sand particles. They designed the apparatus to accommodate three different size volumes of silica sand particles. The sand particles were saturated by water, which occupied all the interstitial space. In the hydrate formation experiments, the subsequent hydrate formation was observed, detected by heat released at the multiple nucleation sites in silica sand bed. In addition, an initial slow growth was followed by a rapid hydrate growth rate of equal magnitude for nearly all experiments until 43-53% of water was converted to hydrate. The final conversions to hydrate between 74 and 98 % were achieved in all experiments.

Kang and Lee (2010) studied the phase equilibrium and formation kinetics of natural gas in meso- and macroporous silica gels. The result indicated that

the hydrate phase equilibrium in porous media was found to shift to the inhibition area than that in the bulk phase (pure water). In addition, the inhibitor effect was observed to be more significant in the meso-sized pore than the macro-sized. The hydrate formation was reached the equilibrium in a short period of time without any mechanical stirrer. Interestingly, the hydrate formation rate of the experiment conducted at 275.2 K was faster than that at 273.2 K even the driving force at 273.2 K is larger than at 275.2 K. They explained that the mass transfer, both viscosity and temperature increased as temperature was increased, leading to increase the mass transfer at higher temperature. Therefore, the hydrate formation was limited due to limitation of mass transfer of gas molecules at low temperature. Furthermore, they stated that a non-stirring method for gas hydrate formation should be considered as a possible option for gas hydrate storage and transportation.

Park and Kim (2010) investigated the effect of multi-walled carbon nanotubes (MWCNTs) in order to increase the rate of methane hydrate formation for the natural gas transport and storage. The experiments were conducted at 274.15 K in a stirred reactor. The results showed that adding 0.004 wt% of MWCNTs to pure water, the amount of gas consumed was 300 % higher than that in pure water; in addition, increasing the subcooling temperature led to decrease the induction time.

The comparative study of CM-95 and CM-100 MWCNTs on methane hydrate formation was performed by Kim *et al.* (2011). The experimental set up was the same as conducted by Park and Kim (2010). The physical length of CM-95 was much shorter than CM-100. They used the various amount of MWCNTs in the experiment and found that 0.004 wt% was the optimum amount of MWCNTS, added in the water for both kinds of MWCNTs. The results showed that the amount of gas consumed during the experiment with the presence of 0.004 wt% of CM-95 was higher than that with CM-100. They concluded that the porous carbon nanotubes acted as a 'seed' during the formation of the hydrate precursors and promoted the nucleation and growth of methane hydrate. In addition, it can also be deduced that a shorter MWCNTs function was better in their role as catalysts.

In 2012, Prasad *et al.* investigated the effect of silica particle on methane hydrate formation. They used the suspension silica (10 wt%) with 50, 150, and 250 μm diameter and the natural clay (bentonite) to compare the effects on

hydrate formation kinetics and efficiency. The experiment conducted in a stirred reactor and cooled down the temperature to 273 K. The results indicated that the induction time and hydrate growth were significantly faster in the suspension of silica with the particle size of 150 and 250 μm compared to pure hydrate. The induction time was slightly longer compared to pure hydrate for the suspensions with 50 μm silica and natural clay sediment. For the hydrate dissociation, the hydrates within fine beads dissociated slowly and the stability of hydrates, measured under the ambient pressure conditions was just up to below melting temperature of ice. In addition, the methane released during the dissociation was almost the same for pure methane hydrates and those formed in silica suspensions. However, it was marginally slower in suspensions of sediments. In comparison with pure methane hydrates, the conversion decreased about 20–30% in silica suspensions, while it was comparable in clay sample.

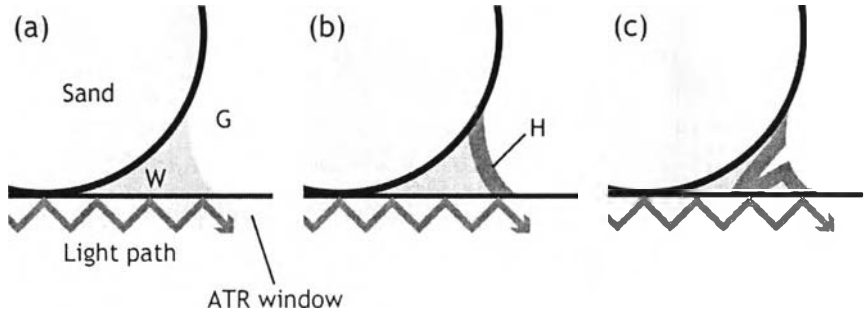

Figure 2.21 Schematic of the relationship between the nature of hydrate and two-step growth during the ATR–IR measurement: (a) before hydrate formation, (b) in the first step of two-step growth, and (c) in the second step of the two-step growth (Jin *et al.*, 2012).

Jin *et al.* (2012) observed the methane hydrate growth in porous media by using attenuated total reflection infared (ATR-IR). The silica sand particles were used in this study. The ATR-IR revealed that the hydrates in porous media grew in two steps. The first step was observed the film-like hydrates at gas-water interface. Later, the hydrate films were collapsed, observed by the visual observation. The second growth step occurred by the fresh liquid-phase H_2O molecules, from the

cracks in the film, entered the hydrate phase as shown in Figure 2.21. In addition, the cracks in the hydrate film were found to change the nature of the hydrate from a film to a cement-like hydrate. They concluded that the two-step growth behavior observed in hydrate formation in porous media showed that the nature of the hydrate in the pores changed during hydrate growth.

Linga *et al.* (2012) enhanced the rate of gas hydrate formation in fixed bed column filled with silica sand compared to a stirred vessel. The hydrate formation experiments were conducted for gas mixtures relevant to natural gas hydrate formation occurred in the earth. The results showed that, at constant experimental temperature and pressure, the rate of hydrate formation in fixed bed column was higher than that in the stirred vessel. In addition, the final gas uptake for the experiments conducted in a fixed bed column was significantly higher than in the stirred vessel. Consequently, a higher percent conversion of water to hydrate was observed in a fixed bed column. However, they stated that the mechanism for the enhancement on the rate of gas hydrate formation in the silica sand bed was not known at that time.

In 2013, Arjang *et al.* used synthesized silver nanoparticles to promote the methane hydrate formation. The aqueous solution with silver nanoparticles was poured in the reactor, and the temperature was decreased from 283.15 K to 275.15 K at 4.7 and 5.7 MPa. The results indicated that the induction time of methane hydrate formation decreased by 85% and 73.9% compared to pure water (380.3 min) for the experimental pressure of 4.7 and 5.7 MPa, respectively. Moreover, the amount of methane consumption increased by 33.7% and 7.4% with the presence of silver nanoparticles at pressure of 4.7 and 5.7 MPa, respectively. They stated that silver nanoparticles had a considerable effect on gas to water ratio of methane hydrate.

Chari *et al.* (2013) investigated the methane hydrate formation and dissociation in nano silica suspension in non-stirred reactor. The experiments were conducted with two set of different silica to water ratio 1:8 and 1:4 at the experimental condition at 7.3 MPa to 11.7 MPa and 267 K. The results showed that the silica to water ratio at 1:4 showed the significant improvement in the overall methane hydrate yield up to 89.4%, while the ratio at 1:8 had the significant amount of unconverted water, which the excess water were remained in the pore water,

causing the lower hydrate yield at about ~ 44%. Moreover, the two steps of methane hydrate dissociation were observed, in the temperature range of 267-273 K and 274-280 K.

Babu *et al.* (2013b) employed the polyurethane foam (PU foam) to enhance the kinetics of clathrate process for the hydrate based gas separation of carbon dioxide from flue gas mixture. The experiment was conducted in the fixed bed reactor using 2.5 mol% propane as a thermodynamic promoter. The mixture of CO_2 (38.1)/H_2 (59.4)/C_3H_8 (2.5) was fed in to the reactor at the operating pressure of 4.5, 5.5, 6.0 MPa and constant temperature of 274.2 K. The results showed that the induction times with the presence of PU foam were shorten significantly. In addition, it can be noted that a higher driving force pressure played an important role to increase the rate of hydrate growth and gas consumption. They stated that PU foam as a porous medium can help convert 54 % of water to the hydrate in two hour of the hydrate formation experiment. Moreover, they showed the mechanism of hydrate formation from water dispersed in interstitial pore space of porous medium as shown in Figure 2.22.

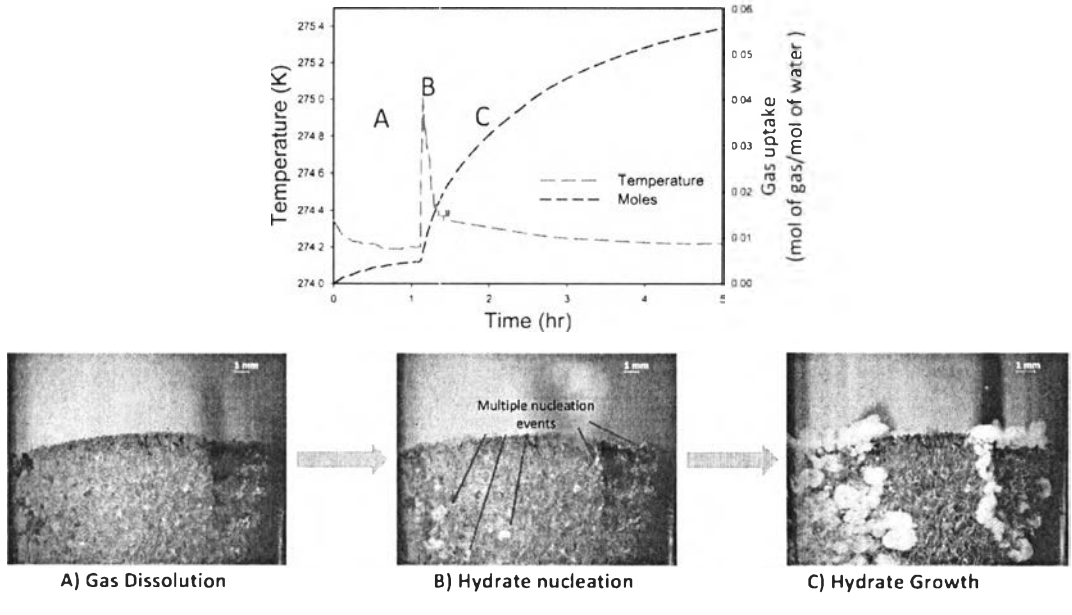

Figure 2.22 Mechanism of hydrate formation from water dispersed in interstitial pore space (Babu *et al.*, 2013b).

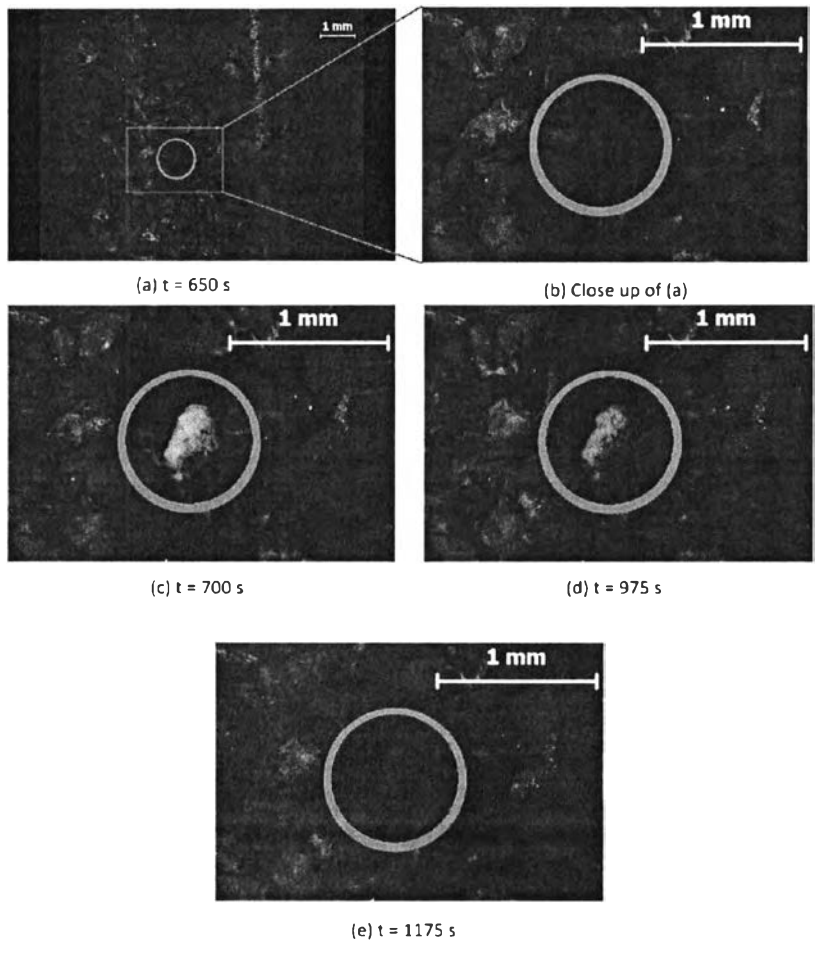

Figure 2.23 Sequential images of the methane hydrate formation in activated carbon with 100% H_2O saturation at 277.15 K and 8.0 MPa (Babu *et al.*, 2013c).

In the same year, Babu *et al.* (2013c) observed the morphology of methane hydrate formation in porous media including silica sand and activated carbon at 8.0 MPa and 277.15 K. The hydrate crystals were observed in the interstitial pore space that available between silica sand particles. Moreover, they observed the formation and dissociation of hydrate crystal on the surface of activated carbon grain in the stable hydrate formation region. They observed the behavior of transient hydrate crystal formation/disoociation in porous media, particularly activated carbon, as shown in Figure 2.23. They postulated that particle size, pore spaces, insufficient wetting of the grains may be the reason for this behavior in the

activated carbon bed. As a result, they concluded that that pore space plays an important role in hydrate formation and dissociation in porous media.

In 2014, Prasad *et al.* enhanced methane storage capacity in gas hydrate formation by using hollow silica. The silica used in the experiment has a mean diameter of 30 – 70 μm and 2.4 m^2/g for its surface area. The fixed amount of hollow silica and water were mixed gently before adding to the reactor and then the temperature was decreased to the desired temperature. The results showed that the methane hydrate formation was associated with silica particles and did not require such vigorous mechanical stirring. The hydrate yield was increased with the increase driving force pressure. In addition, the hydrate yield was higher in silica-water system at moderate higher pressures regardless of non-stirred vessel. That is because of the improvement in surface area of water and gas. The mechanism of methane hydrate formation in hollow silica was still not known. However, the two stages of methane hydrate formation were observed, including the initial nucleation and stable growth under favorable thermodynamics conditions. To increase to volume storage capacity, the silica-water ratio needs to be adjusted. Moreover, the system of hollow silica-water can be reused without a special sample preparation for several hydrate formation-dissociation cycles.

Kim *et al.* (2015) investigated the effects of zeolites on methane hydrate formation. They compared the effect of natural and synthetic zeolites (5A and 13X) on methane hydrate formation and gas storage capacity. They indicated that at the weight fraction of zeolite was below 0.01, the amount of methane gas consumed was proportional to the weight fraction of zeolite. However, at above 0.01 wt%, the gas consumption decreased as the rapid formation of methane hydrate took place at the interfacial area between water and methane gas. The optimum gas consumption appeared to be achieved by 0.01 wt% zeolite in pure water for both natural and synthetic zeolite. This result reflected the effect of it having the smallest particle sizes and largest pores of the tested zeolites. Moreover, the hydrate phase equilibrium of zeolites were slightly shifted to the right of the one with distilled water, indicating that the hydrate formation somewhat easier in the zeolite solutions.

Table 2.2 Gas hydrate consumption reported in literature

References	System	Gas	Pressure (MPa)	Temperature	Stirring rate (rpm)	Water conversion (%)	Hydrate capacity
Khokha *et al.*, 1998	0.1 wt.% Polyvinylpyrrolidone (PVP)	CH_4	3.2	275.5 K	-	Max. 40.99	-
Zhong and Rogers, 2000	242 ppm SDS	C_2H_6	3.89	275.4 K	-	-	156 v/v
Ganji *et al.*, 2007b	1000 ppm trimethyl ammonium bromide (CTAB)	CH_4	8.3	276.2 K	200	-	165 v/v
Partoon *et al.*, 2013	700 ppm SDS	CO_2	35 bar	273.65 K	-	-	~ 0.6 mol/ 500 ml vessel
Sun *et al.*, 2013	300 ppm SDS	CH_4	5.54	274.05	-	-	163 v/v
	300 ppm SDS/500 ppm DPG/ 1.0 wt% CP		5.35				153 v/v
Kumar *et al.*, 2013	230 – 400 mesh silica gel	CO_2	3.55	274 K	-	51.41	-
	230 – 400 mesh silica gel/2000 ppm SDS					53.98	
Hao *et al.*, 2014	Coal/ 242 ppm SDS	CH_4	6	273.15 K	-		179.97 v/v

Table 2.2 Gas hydrate consumption reported in literature (*cont.*)

References	System	Gas	Pressure (MPa)	Temperature	Stirring rate (rpm)	Water conversion (%)	Hydrate capacity
Veluswamy *et al.*, 2015	0 – 1000 ppm SDS	H_2/C_3H_8	8.5	274.2 K	-	-	~ 0.01 mol gas/mol water
Strobel *et al.*, 2006	0.5 – 5.56 mol% THF	H_2	13.8	270 K	-	-	1 wt%
Chari *et al.*, 2012	THF solution: 0.0056 – 0.06 mole fraction	CH_4	10	268 K	500	-	20.7-49.8 %
	t-BuNH2 solution: 0.0056 – 0.06 mole fraction						29.2-48.5 %
Veluswamy *et al.*, 2013	- 1 mol% THF	H_2	12.7	274.4 K	400	3.9	-
	- 2.4 mol% THF		10.8	274.1 K		6.4	
	- 3 mol% THF		8.7	278.2 K		6.7	
	- 3.5 mol% THF		7.9	278.2 K		6.8	
	- 5 mol% THF		8.8	278.2 K		10.7	
Sharma *et al.*, 2014	6.03 mol% THF	CH_4	8.21	285 K	500	-	88 mmol/ 100 ml vessel

Table 2.2 Gas hydrate consumption reported in literature (*cont.*)

References	System	Gas	Pressure (MPa)	Temperature	Stirring rate (rpm)	Water conversion (%)	Hydrate capacity
Veluswamy *et al.*, 2014a	- 3.5 mol% THF - 5.3 mol%THF - 2.0 mol% TBAB - 3.5 mol% TBAB	H_2	12 13 12 13	279.2 K ΔT = 2.2 K 279.2 K ΔT = 2.2 K	400	-	0.169 wt% 0.186 wt% 0.052 wt% 0.035 wt%
Yan *et al.*, 2005	20 – 40 mesh activated carbon	CH_4	9.49	280 K	-	-	140 v/v
Linga *et al.*, 2009	914.1 g silica sand	CH_4	8	7.0 °C 4.0 °C 1.0 °C	-	10.2-11.0 74.1-78.5 79.8-92.4	-
	513.7 g silica sand			4.0 °C		75.9-84.3	
	228.5g silica sand			4.0 °C		75.5-97.8	
Kang and Lee, 2010	Silica gel	Natural gas	5	263 K	-	-	120 v/v
Park *et al.*, 2010	0.004 wt% Multi-walled carbon nanotubes (MWCNTs)	CH_4	n/a	274.15 K	300		~ 0.08 wt%
Kim *et al.*, 2011	- 0.004 wt% MWCNTs (CM-95) - 0.004 wt% MWCNTs (CM-100)	CH_4	n/a	274.15	300		~ 0.08 wt% ~ 0.067 wt%

Table 2.2 Gas hydrate consumption reported in literature (*cont.*)

References	System	Gas	Pressure (MPa)	Temperature	Stirring rate (rpm)	Water conversion (%)	Hydrate capacity
Linga *et al.*, 2012	Fixed bed silica sand Stirred tank Quiescent water	CH_4	8	4.0 °C	- 300 -	94.7 74.1 4.5	-
	Fixed bed silica sand Stirred tank	CO_2	3.1	1.0 °C	- 300	63.5 27.4	-
Chari *et al.*, 2013	250 nm silica powder suspended in water (silica water ratio = 1:4)	CH_4	8.5	263.15 K	-	-	80.0-89.4 %
Babu *et al.*, 2013b	Polyurethane foam (PU foam)	CO_2/H_2 /C_3H_8	6 5.5 4.5	274.2 K	-	58.3-65.0 50.3-55.7 24.3-33.6	-
Prasad *et al.*, 2014	3 g Hollow silica in 15 g water	CH_4	8.82	278 K	-	-	206 v/v
Kim *et al.*, 2015	- 0.01 wt% 5A synthetic zeolite - 0.01 wt% 13X synthetic zeolite - 0.01 wt% Natural zeolite	CH_4	3	274.15 K	300	-	~ 0.115 mol ~ 0.125 mol ~ 0.095 mol